⌘ *Author's Choice*

THE JOURNAL OF BIOLOGICAL CHEMISTRY VOL. 289, NO. 9, pp. 5619–5634, February 28, 2014

A Refined Model for the TSG-6 Link Module in Complex with Hyaluronan

*USE OF DEFINED OLIGOSACCHARIDES TO PROBE STRUCTURE AND FUNCTION**

Received for publication, December 13, 2013 Published, JBC Papers in Press, January 8, 2014, DOI 10.1074/jbc.M113.542357

Victoria A. Higman[‡1], David C. Briggs[§¶1], David J. Mahoney[‡], Charles D. Blundell[¶], Benedict M. Sattelle[¶], Douglas P. Dyer[§¶2], Dixy E. Green[‖], Paul L. DeAngelis[‖3], Andrew Almond[¶], Caroline M. Milner[¶], and Anthony J. Day[§¶4]

From the [‡]Department of Biochemistry, University of Oxford, Oxford OX1 3QU, United Kingdom, [§]Wellcome Trust Centre for Cell Matrix Research, [¶]Faculty of Life Sciences, University of Manchester, Oxford Road, Manchester M13 9PT United Kingdom, and the [‖]Department of Biochemistry and Molecular Biology, Oklahoma Center for Medical Glycobiology, University of Oklahoma Health Sciences Center, Oklahoma City, Oklahoma 73104

Background: The polysaccharide hyaluronan is organized through interactions with the protein TSG-6 during inflammation and ovulation.
Results: NMR spectroscopy on TSG-6 in the presence of defined sugars provided restraints that allowed modeling of a refined hyaluronan/TSG-6 complex.
Conclusion: TSG-6 binding causes bending of hyaluronan that explains its condensation of this polysaccharide.
Significance: This provides novel structural insights into protein-hyaluronan interactions.

Tumor necrosis factor-stimulated gene-6 (TSG-6) is an inflammation-associated hyaluronan (HA)-binding protein that contributes to remodeling of HA-rich extracellular matrices during inflammatory processes and ovulation. The HA-binding domain of TSG-6 consists solely of a Link module, making it a prototypical member of the superfamily of proteins that interacts with this high molecular weight polysaccharide composed of repeating disaccharides of D-glucuronic acid and *N*-acetyl-D-glucosamine (GlcNAc). Previously we modeled a complex of the TSG-6 Link module in association with an HA octasaccharide based on the structure of the domain in its HA-bound conformation. Here we have generated a refined model for a HA/Link module complex using novel restraints identified from NMR spectroscopy of the protein in the presence of 10 distinct HA oligosaccharides (from 4- to 8-mers); the model was then tested using unique sugar reagents, *i.e.* chondroitin/HA hybrid oligomers and an octasaccharide in which a single sugar ring was ^{13}C-labeled. The HA chain was found to make more extensive contacts with the TSG-6 surface than thought previously, such that a D-glucuronic acid ring makes stacking and ionic interactions with a histidine and lysine, respectively. Importantly, this causes the HA to bend around two faces of the Link module (resembling the way that HA binds to CD44), potentially providing a mechanism for how TSG-6 can reorganize HA during inflammation. However, the HA-binding site defined here may not play a role in TSG-6-mediated transfer of heavy chains from inter-α-inhibitor onto HA, a process known to be essential for ovulation.

Hyaluronan (HA)[5] is a linear high molecular weight glycosaminoglycan consisting of repeating disaccharides of β4-D-glucuronic acid (GlcUA) and β3-*N*-acetyl-D-glucosamine (GlcNAc), which is ubiquitously present in the extracellular matrix (ECM) of vertebrate tissues. It plays many different and important biological roles such as providing structural organization to the ECM and regulating cell mobility/activity in the context of both physiological process and disease (1–4). This diversity of function has been suggested to arise via the interaction of HA with various HA-binding proteins (termed hyaladherins) leading to the formation of multimolecular complexes with distinct structural arrangements (or architectures) that likely underlie their different functions (5–7). Most hyaladherins belong to a superfamily of proteins that interact with HA via HA-binding domains (HABD) composed of Link modules, where these have been subdivided into three groups (A, B, and C) on the basis of the size of the HABDs (7, 8). The smallest HABD, denoted as "type A," consists of an individual Link module domain, for which both NMR and crystal structures have been determined for this ~100-amino acid region of human tumor necrosis factor-stimulated gene-6 (TSG-6) (9–11); the Link module was revealed to be a compact structure composed of two β-sheets (I and II) flanked by two α-helices with a fold related to that of the C-type

* This work was supported by Arthritis Research UK Grants 16539, 18472, and 19489 and Medical Research Council Grant G0701180.
⌘ *Author's Choice*—Final version full access.
[1] Both authors contributed equally to this work.
[2] Supported by Biotechnology and Biological Sciences Research Council CASE studentship (BB/D526561/1).
[3] Recipient of an Oklahoma Center for Advancement of Science and Technology Health Research grant.
[4] To whom correspondence should be addressed: Wellcome Trust Centre for Cell-Matrix Research, Faculty of Life Sciences, University of Manchester, Michael Smith Bldg., Oxford Rd., Manchester M13 9PT, UK. Tel.: 44-161-27-51495; Fax: 44-161-27-51505; E-mail: anthony.day@manchester.ac.uk.

[5] The abbreviations used are: HA, hyaluronan; GlcUA, D-glucuronic acid; ECM, extracellular matrix; HABD, hyaluronan-binding domain; IαI, inter-α-inhibitor; HC, heavy chain from IαI; HSQC, heteronuclear single quantum coherence; ITC, isothermal titration calorimetry; Link_TSG6, recombinant Link module from human TSG-6; Tricine, *N*-[2-hydroxy-1,1-bis(hydroxymethyl)ethyl]-glycine.

lectin domain. Currently, the ~150-residue HABD from mouse and human CD44, a major cell surface receptor for HA, provides the only other high resolution structural information for a member of the Link module superfamily (12, 13). In this "type B" HABD, N- and C-terminal sequences flanking the Link module extend the β-sheet structure (adding an additional 4 β-strands to the triple-stranded βI-sheet) to form an extra lobe of structure in intimate contact with the Link module (12); LYVE-1, a related cell surface protein that may function as a HA-binding protein on lymph vessel endothelium and macrophages, is also likely to have a similar extended structure (14). Type C HABDs are composed of contiguous pairs of Link modules (7, 8); however, at present no NMR or crystal structures have been determined. This type of HABD is found in the lectican (aggrecan, brevican, neurocan, and versican) and link proteins (HAPLN1–4), where both modules are necessary for folding and are believed to contribute to HA binding; in some cases an N-terminal immunoglobulin-like fold may also contribute structural stability (15, 16). Although no high resolution data have been obtained for the type C HABDs, homology modeling based on the solution structure of the TSG-6 Link module (in its HA-bound conformation) has provided some useful insights into how the contiguous Link modules may pack together (17).

TSG-6 is a 35-kDa HA-binding protein that is usually expressed in response to proinflammatory stimuli at sites undergoing ECM remodeling (18, 19). It has been hypothesized to be an important protector of tissue structure during inflammation. In this regard, TSG-6 has been found to be chondroprotective in murine models of inflammatory arthritis (see Ref. 20), where its serum concentration correlates well with disease severity (21), and has been found to play a potent inhibitor of osteoclast-mediated bone erosion *in vitro* (22, 23); it is also cardioprotective during myocardial infarction (24), can reduce inflammatory damage to the cornea following injury (25), and can attenuate zymosan-induced peritonitis by decreasing proinflammatory signaling in resident macrophages (26). Given that TSG-6 interacts with a large number of ligands (18, 19), not all of these tissue-protective activities are likely to be mediated via its HA-binding function. Nevertheless, TSG-6 has been shown to enhance/induce the interaction of HA with CD44 on lymphocyte cell lines, which could serve to regulate leukocyte migration by promoting cell adhesion/rolling (27, 28). The recent finding that TSG-6 can directly cross-link HA chains, *i.e.* via the formation of HA-induced TSG-6 oligomers (28, 29), provides a mechanism for this whereby TSG-6/HA complexes could, for example, promote CD44 clustering (27) and/or switch this receptor to its high affinity conformation (13). TSG-6-mediated cross-linking of HA could also serve to remodel ECM, which may contribute to its protective anti-inflammatory activities (27).

In addition to its inflammation-associated functions, it is well established that TSG-6 is essential for female fertility in mice, being required for the assembly of a HA-rich ECM around the oocyte prior to ovulation (30, 31). This process, termed cumulus matrix expansion, has been shown to be reliant on the formation of complexes of HA with heavy chains (HC) from the serum proteoglycan inter-α-inhibitor (IαI) (32–34), where TSG-6 acts as a cofactor and catalyst in the covalent transfer of the HCs onto HA (35); TSG-6-mediated formation of HC·HA also occurs at sites of inflammation (36–38). Covalent HC·TSG-6 complexes act as intermediates in HC transfer (35, 39, 40); this transesterification reaction is preceded by the formation of non-covalent complexes between TSG-6 and IαI that inhibit the HA-binding activity of TSG-6, prevent/disrupt HA-cross-linking, and promote TSG-6 catalytic function (28). The HCs are then transferred from TSG-6 onto HA (35), presumably when the HC·TSG-6 complex and HA interact, although the details of this are not yet fully understood. As well as catalyzing HC·HA production, TSG-6 perhaps may contribute to the stabilization of the cumulus ECM through its simultaneous interaction with HA and pentraxin-3 (41, 42), *i.e.* a multimeric protein (43) that has been implicated as being essential for female fertility (41, 44); IαI HCs also interact with PTX3, providing a possible mechanism for the cross-linking of HC·HA (45).

The HA-binding site in the recombinant Link module of human TSG-6 (termed Link_TSG6) has been defined by site-directed mutagenesis (27, 46, 47) such that functionally important residues were found to line a shallow binding groove when mapped onto Link_TSG6 in its HA-bound solution conformation (10). Two tyrosine residues were concluded to form aromatic stacking interactions with sequential rings in the sugar. This observation along with the polarity of the HA in the binding groove (determined from a comparison of NMR spectra of Link_TSG6 in the presence of HA oligomers of different length; Ref. 10) formed the basis for modeling of Link_TSG6 in complex with an HA octasaccharide (HA_8) (17). In this model only 5 of the 8 sugar rings contacted the protein surface (*e.g.* stabilized by salt bridges in addition to π-stacking interactions), whereas a 7-mer (with GlcUA at either end) was the minimal length of HA oligosaccharide to bind with maximum affinity (10). Furthermore, the oligomer was found to adopt a rather linear conformation in the Link_TSG6/HA_8 model, whereas the more recently determined crystal structure of the murine CD44 HABD in complex with HA_8 showed the HA oligosaccharide to bend around the protein surface (13). Interestingly, NMR spectra of ^{13}C,^{15}N-labeled HA_8 bound to Link_TSG6 contained more than the expected number of peaks, consistent with the octasaccharide being present in more than one conformation (17).

Here we have generated a refined model for the Link module from human TSG-6 in complex with HA by identifying novel restraints based on NMR spectroscopy of Link_TSG6 in the presence of HA oligosaccharides of different length. The model, which was validated by a combination of interaction analysis and NMR experiments with unique sugar reagents (*i.e.* chondroitin/HA hybrid oligomers and an octasaccharide with only one ring isotopically labeled) reveals the HA to make more extensive contacts with the protein surface than thought previously. In particular, the GlcUA at ring 1 of the 8-mer makes a stacking interaction with His^{45} and a salt bridge to Lys^{68} of Link_TSG6, thereby causing the HA to bend around two faces of the Link module; *i.e.* resembling the way HA fits into the binding groove of CD44. This protein-induced conformational perturbation of HA may help explain, at least in part, how TSG-6

can reorganize HA-rich matrices, *e.g.* during inflammation. Furthermore, comparison of the affinities of the interactions of the various HA oligosaccharides with Link_TSG6 with their substrate activities in TSG-6-mediated HC transfer onto HA indicates that the HA-binding surface in the HC·TSG-6 complex is likely to be distinct from that in free TSG-6. Thus the refinement of the Link_TSG6/HA_8 complex described here provides new and important insights into the structure and function of this archetypal HA-binding domain.

EXPERIMENTAL PROCEDURES

Preparation of Protein and Sugar Reagents—Unlabeled and uniformly ^{15}N-labeled Link_TSG6 (residues 36–133 in the TSG-6 preprotein; Ref. 48) were expressed in *Escherichia coli* and purified as described previously (49–51). HA oligosaccharides of defined length (*i.e.* HA_8^{AN} (where A and N correspond to GlcUA and GlcNAc at the non-reducing and reducing termini, respectively), HA_7^{AA}, HA_7^{NN}, HA_6^{AN}, HA_6^{NA}, HA_5^{AA}, HA_5^{NN}, HA_4^{AN}, and HA_4^{NA}) were prepared as described in Blundell and Almond (52), and HA/chondroitin chimeric oligosaccharides (HA_4C_4 and C_4HA_4; with HA_4^{AN} at reducing and non-reducing termini, respectively) were made as before (53, 54). Chondroitin octasaccharides (C_8^{AN}) were made by limited digestion of chondroitin from *Pasteurella multocida* (55) by bovine testicular hyaluronidase (Calbiochem). Size defined oligosaccharides were purified using DEAE HPLC chromatography with an ammonium bicarbonate gradient, as described in Mahoney *et al.* (56). The C_8^{AN} elution position was determined by comparison with HA oligosaccharide standards.

HA_8^{AN}-$^{13}C_6$-GlcUA3 (*i.e.* an HA_8^{AN} oligomer in which the ring 3 GlcUA is uniformly ^{13}C-labeled) was prepared as in DeAngelis *et al.* (54) using UDP-$^{13}C_6$-GlcUA at the single step needed to insert this NMR-active sugar; uniformly labeled UDP-$^{13}C_6$-GlcUA was synthesized by oxidizing UDP-$^{13}C_6$-Glc (Biosupplies Australia Pty Ltd, Victoria, Australia) with the recombinant *E. coli*-derived histidine$_6$-tagged version of the streptococcal UDP-Glc dehydrogenase (57) *in vitro*. The immobilized enzyme reactor method was employed as before, but the intermediate oligosaccharides were purified by gel filtration on a P2 column (Bio-Rad) before and after the addition of the labeled sugar to ensure placement of the $^{13}C_6$-GlcUA3 only at the desired position.

NMR samples were prepared from lyophilized material reconstituted in 10% (v/v) D_2O and 0.02% (w/v) NaN_3; the pH was adjusted to pH 6.0 using NaOH and HCl solutions. In most cases oligosaccharides were added to the ^{15}N-labeled Link_TSG6 protein in a 2-fold molar excess so as to ensure complete binding; HA_4 oligosaccharides were added to ^{15}N-Link_TSG6 in a 10-fold molar excess to reflect the lower binding affinities (10), and HA_8^{AN}-$^{13}C_6$-GlcUA3 was combined with Link_TSG6 at an ~1:3.3 protein:sugar ratio (based on relative peak heights for free and bound sugar (for the C2, C3, C4, and C5 carbons) in the ^{1}H, ^{13}C HSQC described below).

Nuclear Magnetic Resonance—NMR experiments were performed either on a home-built spectrometer at the Oxford Centre for Molecular Sciences with a ^{1}H operating frequency of 599 MHz or on an 800-MHz Bruker instrument at the Department of Molecular Biology and Biotechnology, University of Sheffield. ^{1}H,^{15}N HSQC spectra were recorded at 25 °C (599 MHz) on ^{15}N-labeled Link_TSG6 in the presence of the following HA oligosaccharides: HA_8^{AN} (0.3 mM protein concentration, 1:2 molar ratio of protein to oligosaccharide), HA_7^{AA} (0.3 mM, 1:2), HA_7^{NN} (0.3 mM, 1:2), HA_6^{AN} (1.0 mM, 1:2), HA_6^{NA} (2.0 mM, 1:2), HA_5^{AA} (0.2 mM, 1:1), HA_5^{NN} (0.3 mM, 1:2), HA_4^{AN} (0.3 mM, 1:10), HA_4^{NA} (0.3 mM, 1:10), HA_4C_4 (0.25 mM, 1:1.1), and C_4HA_4 (0.15 mM, 1:1.1). ^{13}C,^{1}H HSQC spectra were recorded at 25 °C (800 MHz) on HA_8^{AN}-$^{13}C_6$-GlcUA3 in the absence (2.5 mM) and presence of unlabeled Link_TSG6 (0.75 mM, 1:3.3). All spectra were processed using NMRPipe (58) and analyzed using Sparky (T. D. Goddard and D. G. Kneller, University of California, San Francisco). The C1-C5 carbons in the free sugar were uniquely assigned using residual $^2J_{CH}$ cross-peaks, where the chemical shift values for the carbons and their associated protons were found to be consistent with those of internal GlcUA residues in the context of a uniformly ^{13}C-labeled HA octasaccharide (*i.e.* with all carbons on all eight sugar residues labeled) analyzed previously (59); although the new peaks, seen in the presence of Link_TSG6, were not independently assigned, the comparison of the ^{13}C and ^{1}H chemical shifts of the new resonances with those of the free sugar allowed their confident identification.

Isothermal Titration Calorimetry—The interactions between Link_TSG6 and HA_8^{NA}, HA_7^{AA}, HA_7^{NN}, HA_6^{NA}, HA_5^{NN}, HA_4C_4, C_4HA_4, and C_8^{AN} oligomers were investigated on a Microcal VP-ITC instrument at 25 °C in 5 mM MES, pH 6.0, as described previously (46, 47). Oligosaccharide solutions (0.21–0.32 mM) were added to the protein (0.015–0.029 mM) in 26 × 5-μl injections. The Origin software package was used to fit the data to a one-site model by nonlinear least squares regression after subtracting the heats resulting from the addition of oligosaccharide into buffer alone. Affinities/thermodynamics for the interactions were determined by averaging the results from three separate experiments. ITC data (including previously unpublished thermodynamic values) for HA_{10}^{AN}, HA_8^{AN}, HA_6^{AN}, and HA_5^{AA} were taken from Blundell *et al.* (10), and minor numerical errors were corrected; in the case of HA_7^{AA}, only values from the present study were used.

Model Building—Models of the Link_TSG6/HA_8^{AN} complex were built as described previously (17) except for the addition of two extra structural restraints; the coordinates of the 20 lowest energy structures determined for the bound conformation of Link_TSG6 were used (PDB 1o7c; Ref. 10) and were kept fixed throughout, whereas all the saccharide rings were modeled in the $^4C_1$ conformation. On the basis of the observed HA oligomer-induced NMR shift changes (determined here) as well as recent pH dependence and mutagenesis data (60), an additional 3.5 Å ring-stacking interaction between the ring 1 GlcUA and His^{45} was introduced. This restraint caused distortions in some models that were removed in all but two of the 20 lowest energy structures upon the addition of a further restraint between the ring 4 GlcNAc methyl group and the Ile^{61} side chain (*i.e.* present within a hydrophobic pocket on the Link module surface; Ref 10).

Heavy Chain Transfer Assays—The ability of HA oligosaccharides (HA_{14} (control), HA_8^{AN}, HA_8^{NA}, HA_7^{NN}, HA_7^{AA}, HA_6^{AN}, HA_6^{NA}, HA_5^{AA}, HA_5^{NN}, HA_4^{AN}, and HA_4^{NA}) to act as

substrates for the covalent attachment of HCs (from IαI) was determined using the assay described before (35); recombinant human TSG-6 was expressed in *Drosophila* Schneider-2 cells and purified as described previously (61), and IαI (a kind gift from Professor Erik Fries) was purified from human serum (62). Briefly, IαI (320 μg/ml), TSG-6 (80 μg/ml), and HA oligosaccharides (molar equivalents of the HA_{14} control at 40 μg/ml) were incubated in 20 mM HEPES-HCl, pH 7.5, 150 mM NaCl, 5 mM $MgCl_2$ in a total volume of 25 μl for 2 h at 4 °C. Samples (15 μl) were then run on 10% (w/v) Tris-Tricine/SDS-polyacylamide gels after reduction with 5% (v/v) β-mercaptoethanol in SDS protein sample buffer (5 min at 100 °C) and stained using Coomassie Blue. All HA oligosaccharides were analyzed at least three times, and the relative intensities of the various HC·HA_n species formed (~85 kDa) were determined by eye.

RESULTS

Defining the Position of HA within the Binding Groove of the TSG-6 Link Module—In a previous study we generated a model of the TSG-6 Link module (Link_TSG6) in complex with an HA_8^{AN} oligosaccharide (17). This model was based in part on the solution structure of Link_TSG6 in the presence of HA_8^{AN} (*i.e.* in its HA-bound conformation) and on the comparison of ^1H,^{15}N HSQC spectra of ^{15}N-labeled Link_TSG6 in the presence of unlabeled HA oligosaccharides of different length (10); *i.e.* HA_{10}^{AN}, HA_8^{AN}, HA_7^{AA}, HA_6^{AN}, HA_5^{AA}, or HA_4^{AN}. The spectra were very similar and showed the different oligosaccharides to be lying in the same binding site on Link_TSG6. A few discrete differences in the spectra were used to deduce the orientation and approximate positioning (register) of the octasaccharide on the Link_TSG6 HA-binding surface. This and other information was used to create a model of the Link_TSG6/HA_8^{AN} complex (17).

Since then a new set of HA oligosaccharides that contain a GlcNAc at their non-reducing termini have become available (52). Further ^1H,^{15}N HSQC spectra of ^{15}N-labeled Link_TSG6 with these new HA oligosaccharides were recorded so as to test the previous model. These were found to be very similar to the previous NMR spectra, indicating that the oligosaccharides are all binding to Link_TSG6 at the same site. However, for several residues key differences in the chemical shift values of their backbone amide resonances were seen. Fig. 1 shows overlays of the ^1H,^{15}N HSQC spectra for some of these residues in Link_TSG6 when it is in complex with the 10 different HA oligosaccharides possible for HA_4 to HA_8 (*i.e.* including the 5 new oligomers described under "Experimental Procedures").

Two distinct sets of peaks are seen within the spectra of Val^{62}. One arises from Link_TSG6 in complex with HA_8^{AN}, HA_7^{AA}, and HA_6^{AN} (denoted by *II* on Fig. 1), and the other arises from HA_6^{NA} and the four HA_5 and HA_4 oligosaccharides (*peak I*); HA_8^{NA} and HA_7^{NN} have peaks in both positions. Thus a particular chemical shift perturbation is seen at Val^{62} for all oligosaccharides that have a GlcUA at position 1 (Fig. 2). The spectra also provide evidence for HA_8^{NA} and HA_7^{NN} binding to Link_TSG6 in two different registers, *e.g.* with the reducing terminal ring of HA_7^{NN} placed at either position 8 (analogous to HA_8^{AN}) or position 6 (analogous to HA_6^{AN}); two registers were seen previously for HA_{10}^{AN} (10).

The spectra for Lys^{63} contains three main peak clusters: peak III (on Fig. 1) arising from HA_8^{NA}, HA_8^{AN}, HA_7^{NN}, HA_7^{AA}, and HA_6^{AN}, peak IV from HA_8^{NA}, HA_7^{NN}, HA_6^{NA}, HA_5^{NN}, and HA_4^{NA}, and peak V from HA_5^{AA} and HA_4^{AN}. These data show that the environment of Lys^{63} is sensitive to the presence or absence of a GlcUA ring at position 1 as well as to the presence or absence of a GlcNAc ring at position 2 (see Fig. 2). The double register of HA_8^{NA} and HA_7^{NN} is again apparent (being present in peaks III and IV; Fig. 1), and the influence of the extra GlcNAc ring at the non-reducing terminus in one of these conformations is also visible in the Lys^{63} shift map by the slight downfield shift of the peak relative to the other resonances in both the ^1H and ^{15}N dimensions. Furthermore, small exchange peaks show that the sugar moves between one register and the other on the millisecond timescale of the NMR experiment. His^{45} gives rise to a similar pattern of resonances to Lys^{63}, *i.e.* with three sets of peaks (VI, VII, and VIII) but with shifts of smaller magnitude; the NH resonance for Cys^{47} is also perturbed in a similar manner (data not shown).

The orientation of the HA oligosaccharides can be inferred from the shift perturbations for Ala^{49} and Tyr^{78} (Fig. 1). Both draw a distinction between oligosaccharides containing a GlcUA ring at position 7 (HA_8^{AN}, HA_8^{NA}, HA_7^{NN}, HA_7^{AA}, HA_6^{NA}, HA_5^{AA}, *e.g.* corresponding to peak IX on Fig. 1) and those terminating with a GlcNAc at position 6 (HA_7^{NN}, HA_6^{AN}, HA_5^{NN}, HA_4^{AN} corresponding to peak X). In addition, the Ala^{49} shift map shows distinct peaks for HA_5^{AA}, HA_4^{NA}, and HA_4^{AN}. These peaks may arise from the lower binding affinity of these oligosaccharides (see ITC results below) that allows greater flexibility to the β4-β5 loop in Link_TSG6 (10) and a consequent averaging of chemical shifts.

Identifying New Interactions between HA and the TSG-6 Link Module—The ^1H,^{15}N HSQC spectra of Link_TSG6 with the new HA oligomers are all consistent with the previous binding model (17), including the orientation and register of the oligosaccharides within the Link module binding groove (summarized in Fig. 2). However, this comparative shift map analysis has identified novel perturbations to His^{45}, Val^{62}, and Lys^{63} when ring positions 1 or 2 are occupied. Thus, these residues are likely to be involved in protein-oligosaccharide interactions or at least be in close proximity to the bound HA. This might explain how HA_7^{NN} is able to bind in two registers and why HA_6^{AN} binds at positions 1–6 rather than 3–8. In both cases the salt bridge at Arg^{81} is omitted in favor of binding at positions 1 and 2, suggesting that the sugar is in fact able to form favorable interactions with the protein at these points. In this regard, inspection of the Link_TSG6 structures in the presence and absence of HA_8^{AN} (10, 11) shows that His^{45} lies flat on the surface of the protein when it is bound to HA_8^{AN}, in contrast to the free protein, where it is at right angles to the surface and partially buried. Thus a ring stacking interaction between this residue and a sugar ring would be possible, where this is likely to be affected by the charge state of the histidine ring; histidine side chains have been shown to be able to make π-stacking interactions with both protein and non-protein ligands (63, 64). It has been shown that the Link_TSG6/HA interaction is pH-dependent and that one of the contributing factors to this is the protonation/deprotonation of His^{45}, the deprotonated form

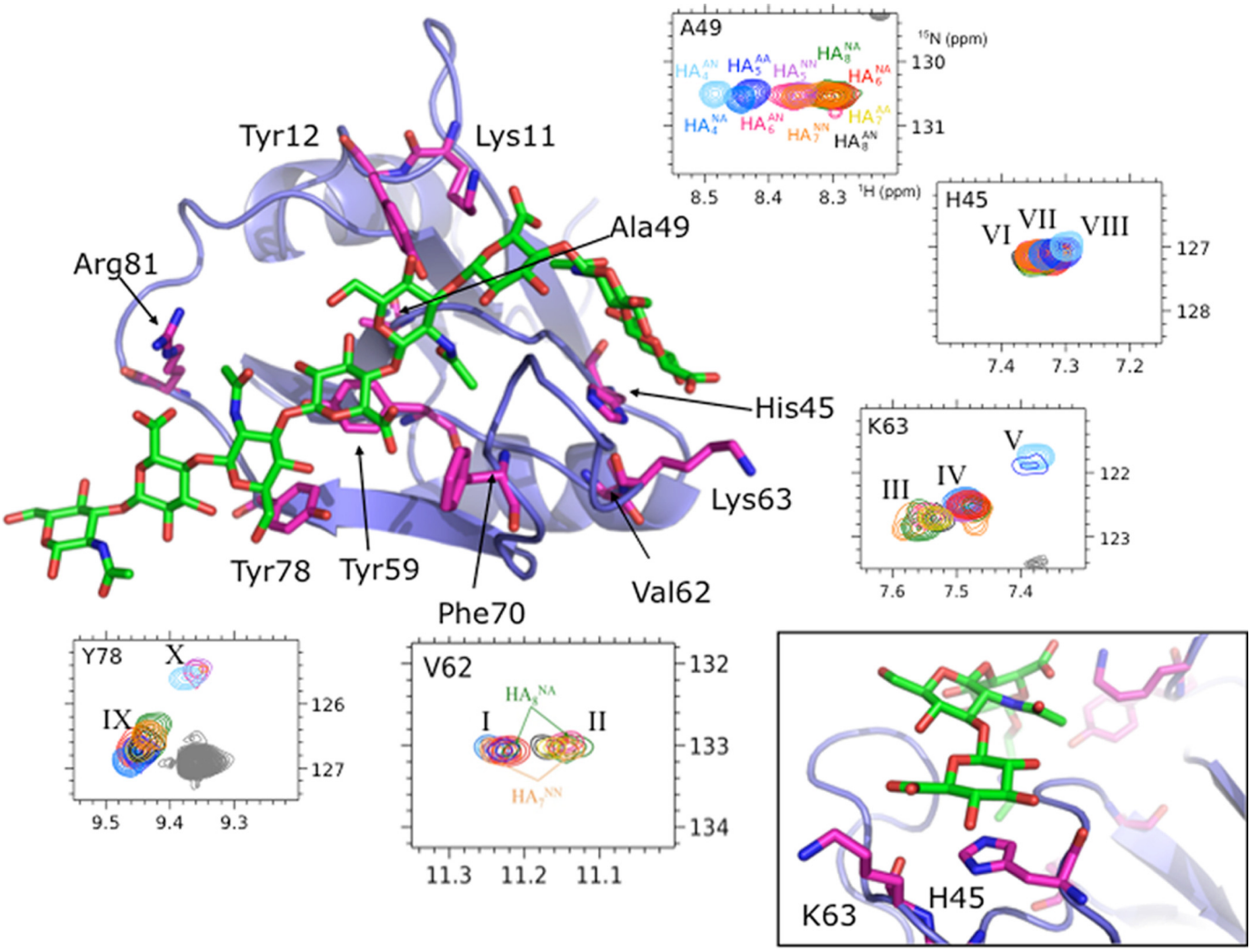

FIGURE 1. **Use of NMR spectroscopy to refine the model of the Link_TSG6/HA_8^{AN} complex.** ^{1}H,^{15}N HSQC NMR spectra were acquired for ^{15}N-labeled Link_TSG6 in the presence of 10 different HA_n oligosaccharides. Regions of these spectra are shown for backbone amide resonances (color-coded as defined for the Ala[49] shift map) that experience differential perturbations compared with HA_8^{AN}; distinct sets of resonances are sub-grouped accordingly using Roman numerals. The positions of these differentially perturbed residues (side chain carbons in *pink*) are shown on the Link_TSG6 NMR structure (*blue ribbon*) in its HA_8^{AN}-bound conformation (PDB accession code 1o7c; Ref. 10); the lowest energy structure from the family of 20 structures is used here and in all other figures. HA_8^{AN} (carbons are in *green*) is displayed in a representative Link_TSG6-bound conformation, *i.e.* as determined in this study from the refined model of the Link_TSG6/HA_8^{AN} complex; this particular HA_8^{AN} conformer is used in all subsequent figures. The *inset* (*bottom right corner*) shows the ring stacking interaction between the non-reducing terminal glucuronic acid (ring 1) and His[45], inferred from the refined Link_TSG6/HA_8^{AN} model, and the proximity of this sugar ring to Lys[63], with which it may form a salt bridge; in this particular model the Lys[63] is not in the correct orientation to make such an ionic interaction.

being required for maximal binding (60); the pK_a of His[45] is 5.7 in the HA_8^{AN}-bound protein, and this residue was demonstrated to be uncharged at pH 6.0 (*i.e.* under the conditions used here). Furthermore, mutation of His[45] to serine causes a greater than 2-fold reduction in the binding affinity (60).

New Model for the Link_TSG6/HA_8^{AN} Complex—We have now refined the model of the Link_TSG6/HA_8^{AN} complex to include a ring-stacking interaction between His[45] and ring 1 of the HA octasaccharide (see "Experimental Procedures"). Although in the initial models generated, the HA was always positioned within the expected binding groove on the surface of the protein, in some cases bond distortions were observed, and the sugar passed through the protein behind the Cys[47]-Cys[68] disulfide bridge. To prevent these implausible conformations, a restraint was introduced between the *N*-acetyl methyl group of ring 4 and the side chain of Ile[61]. This fixed ring 4 of HA in the position observed previously where the Me group is buried in a small hydrophobic pocket present on the surface of the protein in the HA-bound structure (PDB 1o7c; Ref. 10). Two of the final 20 models generated still contained distorted bonds, and a further eight contained HA glycosidic bond angles well outside the most favored regions of the Φ/Ψ space plot determined previously for HA (65–67); therefore, these models (Fig. 3; *triangles*) were rejected. As can be seen from Fig. 4, the remaining 10 models overlay well (denoted by *circles* on Fig. 3) and contain only two HA glycosidic bond angles outside the favored regions. Thus, this family of 10 related structures constitutes the refined model of the Link_TSG6/HA_8^{AN} complex, where the HA conformer in association with the lowest energy protein solution structure (*i.e.* from the family of models in Ref. 10) is shown in Figs. 1 and 3. The new model is very similar to that in Blundell *et al.* (17) for rings 3–8; however, rings 1–2 now make close contact with the protein surface via interactions with His[45] and Lys[63] (see Fig. 1). These new interactions are possible

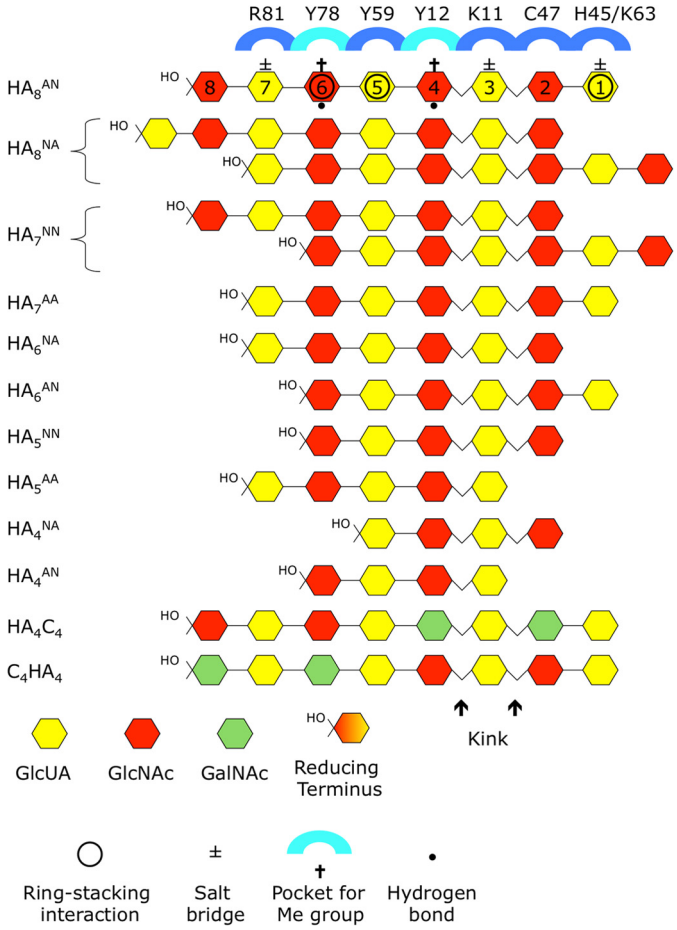

FIGURE 2. **Schematic showing how oligosaccharides are accommodated in HA-binding groove of Link_TSG6.** Ten HA oligomers ranging in length from tetra- to octasaccharides and two-hybrid (chondroitin/HA) 8-mers were used in the current study. Differences in NMR chemical shift perturbations of Link_TSG6 in the presence of these oligomers were used to determine their orientation and register within the HA-binding site as well as their positions relative to key amino acids that mediate the interaction. This analysis indicates that the HA_8^{AN} oligosaccharide interacts with Link_TSG6 through a combination of ionic interactions (*i.e.* between Lys^{11}, Lys^{63}, and Arg^{81} and rings 3, 1, and 7 of the sugar, respectively), ring-stacking interactions (between His^{45}, Tyr^{59}, and Tyr^{78} and rings 1, 5, and 6), hydrogen bonds (between the hydroxyls of Tyr^{12} and Tyr^{78} and rings 4 and 6), and accommodation of the methyl groups from rings 4 and 6 (GlcNAc sugars) in hydrophobic pockets at the bottom of the binding groove; rings 2 and 3 wrap round the Cys^{47}-Cys^{68} disulfide, making van der Waals contacts (where Cys^{47} is in close proximity to ring 2), and the Phe^{70} may also make an occasional ring stacking interaction with ring 4 (not shown). From modeling of the HA_8^{AN} into the structure of Link_TSG6 (determined in its HA_8^{AN}-bound conformation), it is apparent that the oligosaccharide must kink (*i.e.* at the glycosidic bond between rings 2 and 3) to become fully accommodated within the binding site.

due to a pronounced kink in the HA chain involving the glycosidic bond between rings 2–3 and 3–4. However, it should be noted that the Φ/Ψ angles adopted all have energetically favored conformations (65–67); the Φ angles in the selected 10 models, which all have a restricted range of values (see Fig. 3), indicate that these sugar rings are adopting a non-exoanomeric conformation. It is likely that this conformation is stabilized by the binding of HA to the Link module, as has been seen for other carbohydrate-protein interactions (see Ref. 68). As described in the following sections, we then tested the validity of this Link_TSG6/HA_8^{AN} model using a combination of ITC and NMR analyses.

Interactions of HA Oligomers with Link_TSG6—ITC was used to determine the affinities for the interactions between Link_TSG6 and the new HA oligosaccharides (Table 1); representative ITC plots for HA_8^{NA}, HA_7^{NN}, and HA_5^{NN} are illustrated in Fig. 5. Together with the data determined previously for the other oligomers (see Table 1; Ref. 10), it can be seen that HA_8^{AN} and HA_{10}^{AN} bind with essentially identical affinity and that both 7-mers have only slightly weaker binding (~70% of HA_8^{AN}); the K_d for the HA_7^{NN} interaction will be an average of the affinities for the two different binding modes of this oligomer (Fig. 2), which as noted above exchange on the millisecond timescale, making it impossible to dissect the individual affinities corresponding to the two registers. However, the 5- and 6-mers display considerably lower affinity (ranging from ~5–13% of HA_8^{AN}) revealing that these oligomers all bind suboptimally to the TSG-6 Link module. From the schematic in Fig. 2, it can be seen that HA_7^{AA} is the shortest HA oligosaccharide to completely fill the HA-binding site as defined in the refined model of the Link_TSG6/HA_8^{AN} complex. Unexpectedly, the alternative 8-mer (HA_8^{NA}) binds to Link_TSG6 with an ~2-fold higher affinity than HA_8^{AN}; as for HA_7^{NN}, this oligomer is present in two different registers, where the 8-mer with a GlcUA at position 1 is the most abundant species (based on NMR peak ratios for Val^{62}; see Fig. 1), and therefore, this binding mode will dominate the ITC-derived data. From the ΔH and $T\Delta S$ values (Table 1), it is apparent that this increase in affinity is due to a more favorable entropy. Why this oligomer should bind more tightly than HA_8^{AN} (and HA_{10}^{AN}) is not clear, and the analyses of the thermodynamic parameters in Table 1 (which have been included here for completeness) are difficult to interpret; deciphering differences in enthalpic and entropic contributions in protein-ligand interactions is far from straightforward (see Ref. 69).

Interaction of Chondroitin/HA Hybrid Oligomers with Link_TSG6—Hybrid GAG polymers can be made using the HA synthase, PmHAS, and the chondroitin synthase, PmCS, from the Gram-negative bacterium *P. multocida* (54). Here two such chimeric oligosaccharides, HA_4C_4 and C_4HA_4, were used to test the validity of the refined Link_TSG6/HA_8^{AN} model. Given that the disaccharides of unsulfated chondroitin (-β1,4-GlcUA-β1,3-GalNAc-) and HA (-β1,4-GlcUA-β1,3-GlcNAc-) differ only by the placement of one OH group (at the 4 position), it seemed likely that these oligosaccharides would be accommodated within the Link module HA-binding groove but that any small differences in their binding compared with HA_8^{AN} might prove informative. In this regard, ^1H,^{15}N HSQC spectra of Link_TSG6 in the presence of HA_4C_4 or C_4HA_4 were found to be very similar to that of the Link_TSG6/HA_8^{AN} complex (Fig. 6); thus, the hybrid oligosaccharides both bind to Link_TSG6 at the same site as the HA oligomers, as was anticipated. The differences seen in the chemical shifts induced in Link_TSG6 by HA_4C_4 and C_4HA_4, in comparison to HA_8^{AN}, are consistent with the orientation and positioning of HA in the refined (and original) models.

HA_4C_4 interacts with Link_TSG6 with an essentially identical affinity to that of HA_8^{AN} (~91%); this interaction has an enthalpy term that is 1 kcal·mol^{-1} less favorable than for HA_8^{AN}, which is compensated by a more favorable entropy (see

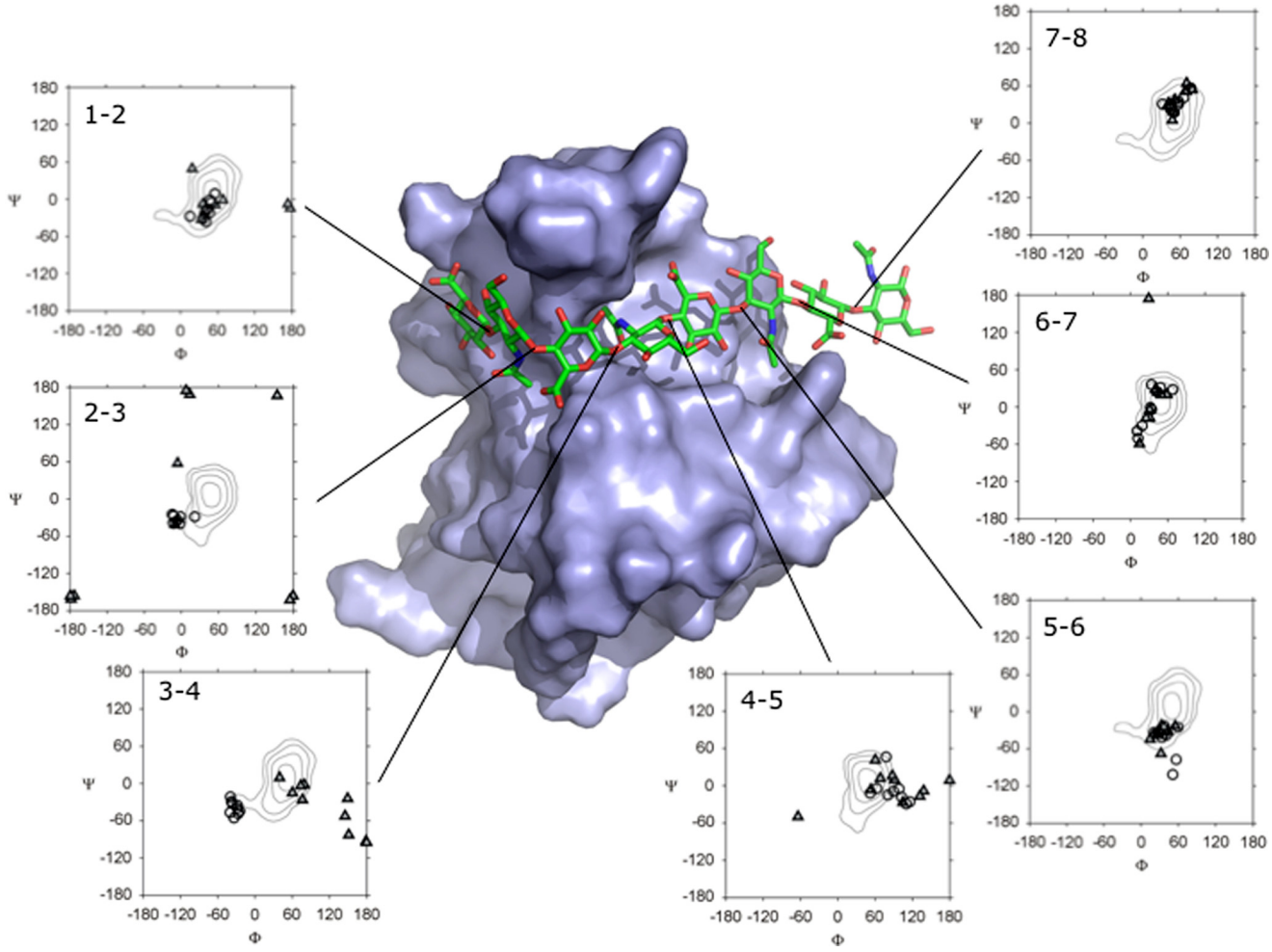

FIGURE 3. **Glycosidic bond angles for family of 20 models determined for Link_TSG6/HA_8^{AN} complex.** The Link_TSG6 protein structure is shown as a solvent-accessible surface with the modeled HA_8^{AN} oligosaccharide in a representative conformation (see legend to Fig. 1). Φ/Ψ space plots are displayed for the 7 glycosidic linkages (*i.e.* between rings 1 and 2 (1–2), 2 and 3 (2–3), etc.) in the final 20 models. Glycosidic bond angles are denoted by either *circles* for the 10 best models, *i.e.* that lie within the most favored regions of the Φ/Ψ space plot or by *triangles* for the 10 models that were rejected (*i.e.* based on the presence of distorted bonds or glycosidic angles outside these favorable regions); the contour plots describe the preferred conformations predicted by molecular dynamic simulations for HA in solution (61–63). The contours levels shown are at 2 kcal/mol intervals above the lowest energy.

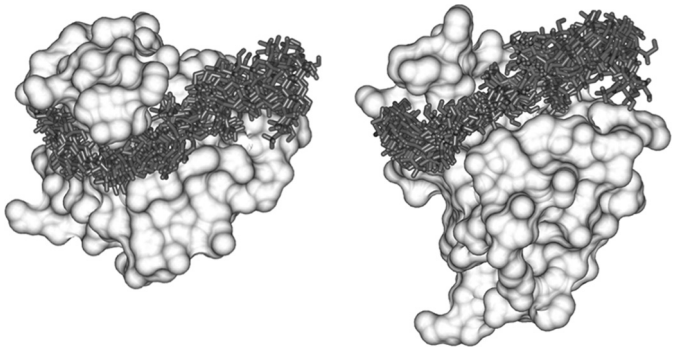

FIGURE 4. **Family of models of the Link_TSG6/HA_8^{AN} complex.** Shown is an overlay of 10 selected models where the *left* and *right hand* images are rotated through ~90° (around the *x* axis) relative to one another. The HA conformers (*sticks*) are displayed on the lowest energy protein structure (shown as a solvent-accessible surface).

Table 1). In the case of HA_4C_4 there are only a few chemical shift perturbations above the threshold that were chosen as significant (*i.e.* 0.05 and 0.2 ppm for H^N and N^H, respectively). The three largest N^H shift changes (see Fig. 6) correspond to Lys^{63}, Cys^{68}, and Gly^{69}, and three of the significantly perturbed H^N (*i.e.* for Cys^{47}, Ala^{49}, and Lys^{63}) are all in close proximity to the sugar rings 1–4 in the Link_TSG6/HA_8^{AN} model (*colored orange* on Fig. 7), which includes GalNAc at rings 2 and 4 in this hybrid oligomer. Ring 2 lies above the disulfide bond formed between Cys^{47} and Cys^{68} (that are both perturbed), and Ala^{49} and Gly^{69} are adjacent to ring 4, where these subtle perturbations can be readily explained by the change in position of the C4 hydroxyls from equatorial to axial; for example, Gly^{69} forms part of the specificity pocket occupied by the *N*-acetyl moiety of ring 4 (17), where a change in orientation of this group, *e.g.* caused by a steric clash between Tyr^{12} and the C4-OH in the hybrid oligomer (and the loss of a hydrogen bond between the hydroxyl Hη proton of Tyr^{12} and the C4-OH of HA; Ref. 10), could induce the large chemical shift perturbation observed. The only other significant shift perturbation to an amide nitrogen is in Tyr^{33}, which is distant from the HA-binding groove, where we have shown previously that this atom is sensitive to changes in salt strength (70). Therefore, it seems plausible that this perturbation results from the presence of counter ions in this preparation; the shift change observed for the H^N of Tyr^{16} (with both hybrid oligosaccharides) may also result from minor

TABLE 1
Binding and thermodynamic constants for the interaction of Link_TSG6 with oligosaccharides of defined size as determined by ITC

Oligosaccharide	*N*	K_b	ΔG	ΔH	$T\Delta S$	% HA_8^{AN}
		$\times 10^5$ M^{-1}	kcal·mol^{-1}	kcal·mol^{-1}	kcal·mol^{-1}	
HA_{10}^{AN} [a]	1.01 ± 0.00	61.2 ± 14.4	−9.19 ± 0.14	−7.57 ± 0.67	1.62 ± 0.60	113
HA_8^{NA} [b]	0.97 ± 0.01	102.3 ± 3.78	−9.56 ± 0.02	−6.90 ± 0.03	2.66 ± 0.03	188
HA_8^{AN} [c]	1.00 ± 0.01	54.3 ± 5.55	−9.16 ± 0.07	−8.01 ± 0.35	1.15 ± 0.38	100
HA_7^{NN} [b]	0.93 ± 0.03	36.8 ± 0.84	−8.96 ± 0.01	−11.26 ± 0.34	−2.30 ± 0.33	67.8
HA_7^{AA} [b]	0.98 ± 0.04	39.2 ± 1.71	−9.00 ± 0.02	−10.03 ± 0.47	−1.03 ± 0.45	72.2
HA_6^{NA} [b]	0.89 ± 0.06	7.0 ± 0.53	−7.96 ± 0.04	−11.29 ± 0.28	−3.33 ± 0.24	12.9
HA_6^{AN} [a]	1.00 ± 0.01	5.8 ± 1.64	−7.77 ± 0.16	−5.40 + 0.11	2.37 ± 0.12	10.6
HA_5^{NN} [b]	1.03 ± 0.02	5.9 ± 0.34	−7.87 ± 0.03	−15.25 ± 0.35	−7.38 ± 0.38	10.8
HA_5^{AA} [a]	1.01 ± 0.02	2.9 ± 1.60	−7.35 ± 0.37	−7.06 ± 1.33	0.30 ± 0.97	5.3
HA_4^{AN} [d]	1	0.22				0.4
C_4HA_4 [b]	0.91 ± 0.08	33.0 ± 5.44	−8.87 ± 0.11	−7.65 ± 0.10	1.22 ± 0.10	60.8
HA_4C_4 [b]	0.96 ± 0.06	49.7 ± 4.47	−9.13 ± 0.05	−7.02 ± 0.25	2.11 ± 0.29	91.4
C_8 [b]	0.97 ± 0.07	11.0 ± 1.98	−8.22 ± 0.11	−6.27 ± 0.39	1.95 ± 0.28	20.2

[a] Stiochiometry (*N*) and K_b values were taken from Blundell *et al.* (10), and ΔG, ΔH, and $-T\Delta S$ were calculated from these data; minor corrections to values for HA_{10}^{AN}, HA_6^{AN}, and HA_5^{AA} quoted in (10) are based on reanalysis of data.
[b] Mean values were determined here from three separate ITC experiments (±S.E.).
[c] Mean values determined from eight datasets taken from (10) and two additional ITC experiments (±S.E.).
[d] Mean value (taken from Blundell *et al.* (10)) estimated from NMR assuming a 1:1 stoichiometry.

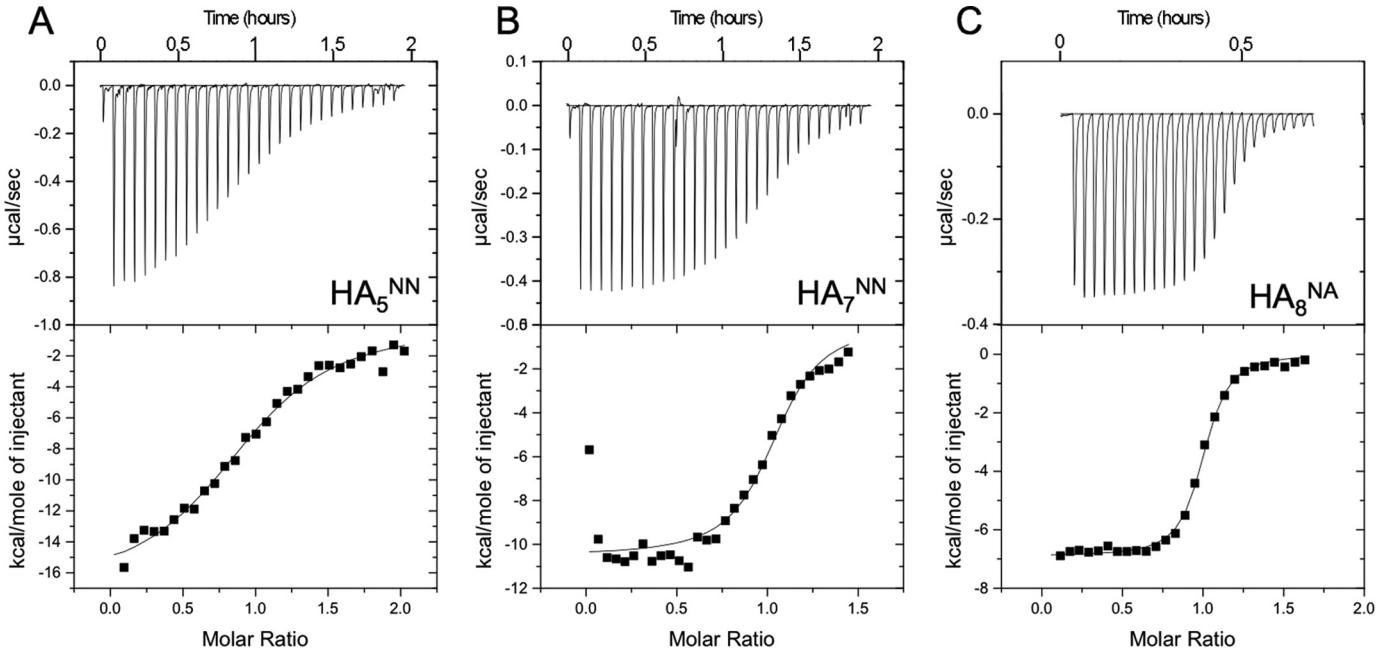

FIGURE 5. **ITC analysis of the interaction between Link_TSG6 and HA oligomers of different length.** Representative titration plots for the binding of Link_TSG6 to HA_5^{NN} (*A*), HA_7^{NN} (*B*), and HA_8^{NA} (*C*) were determined from the integrated raw data after subtraction of heats of dilution of injectant (*i.e.* oligosaccharide); protein concentrations of 29, 15, and 15 μM and HA concentrations of 318, 210, and 240 μM were used, respectively. For each titration the data are fit by least squares regression to a one-site model, where the derived dissociation constants and stoichiometries are presented in Table 1.

changes in buffer composition. Therefore, the chemical shift differences seen in the Link_TSG6 NMR spectra in the presence of HA_4C_4 compared with HA_8^{AN} are consistent with the orientation of HA in the refined and original models.

The C_4HA_4 oligomer binds with a somewhat lower affinity to Link_TSG6 compared with that of HA_8^{AN} (~61%); *i.e.* due to a decreased enthalpy (see Table 1). The generally small perturbations observed in the $^1H,^{15}N$ HSQC are more widespread than for HA_4C_4 described above (Fig. 7). Although Gly^{79} and Arg^{81} (which have perturbed N^H) are located near to sugars 5–8 (colored *pink* in Fig. 7), none of the other differentially affected residues are in close proximity to rings 6 and 8. However, the majority of these amino acids are in regions of Link_TSG6 that have been found previously to undergo significant conformational changes on HA binding (*e.g.* β1-α1 loop (Tyr^{12}) and β4-β5 loop (Cys^{68}, Gly^{71}, Thr^{73} and Gly^{74})) (10). It seems likely, therefore, that the conformational change induced by C_4HA_4 is slightly different from that caused by HA_8^{AN}, *i.e.* due to a subtle alteration in the position of this hybrid oligomer within the binding groove. This might disrupt the hydrogen bond between the side-chain OH group of Tyr^{78} (that has a slowly exchanging Hη in the presence of HA_8^{AN}; Ref. 10) and the C4 OH group on ring 6, and this could give rise to the lower affinity for C_4HA_4. This conformational difference may also explain the perturbation to H^N of Ala^{49} that lines the specificity pocket occupied by ring 4. Furthermore, the slight reduction in binding affinity and the lack of major chemical shift perturbations seen with the C_4HA_4 oligomer indicate that the stacking interaction between Tyr^{78} and ring 6 can still take place when a GlcNAc is replaced by a GalNAc. This is consistent with the revised (and original) Link_TSG6/HA_8^{AN} models, in which the face of the GlcNAc of ring 6 that stacks against the side chain of Tyr^{78} is correctly

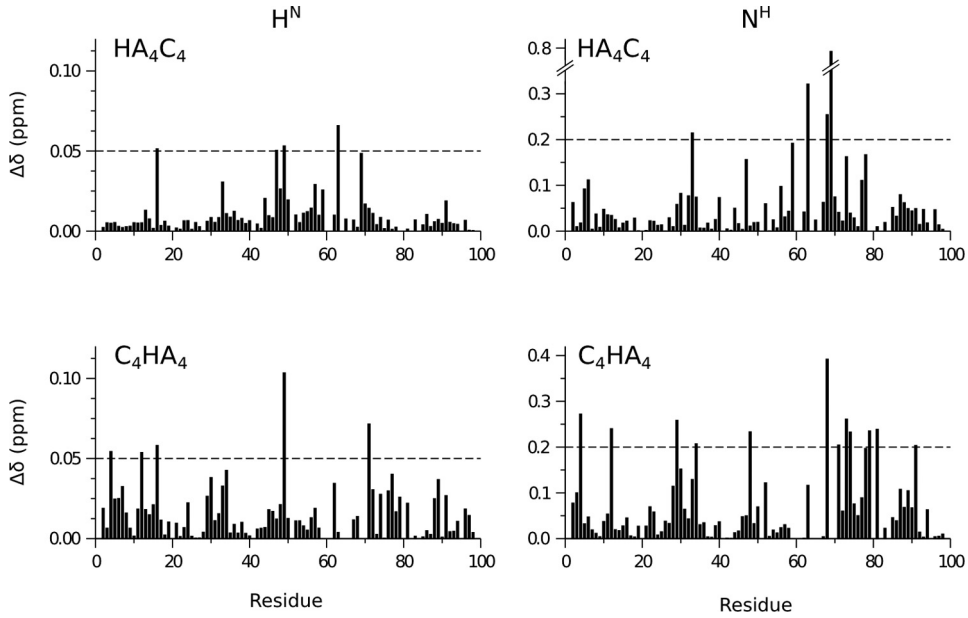

FIGURE 6. **Chemical shift perturbations in Link_TSG6 caused by hybrid oligomers HA_4C_4 and C_4HA_4 relative to HA_8^{AN}.** *Bar charts* show the absolute chemical shift differences ($\Delta\delta$) between Link_TSG6 in the presence of HA_8^{AN} compared with HA_4C_4 (*top*) or C_4HA_4 (*bottom*). The $\Delta\delta$ values are shown for the backbone amide protons (H^N) and nitrogens (N^H) that were derived from ^1H,^{15}N HSQC spectra acquired on ^{15}N-labeled Link_TSG6, where the *horizontal dotted lines* represent the arbitrary threshold levels chosen to indicate a significantly perturbed resonance ($H^N > 0.05$ ppm; $N^H > 0.20$ ppm).

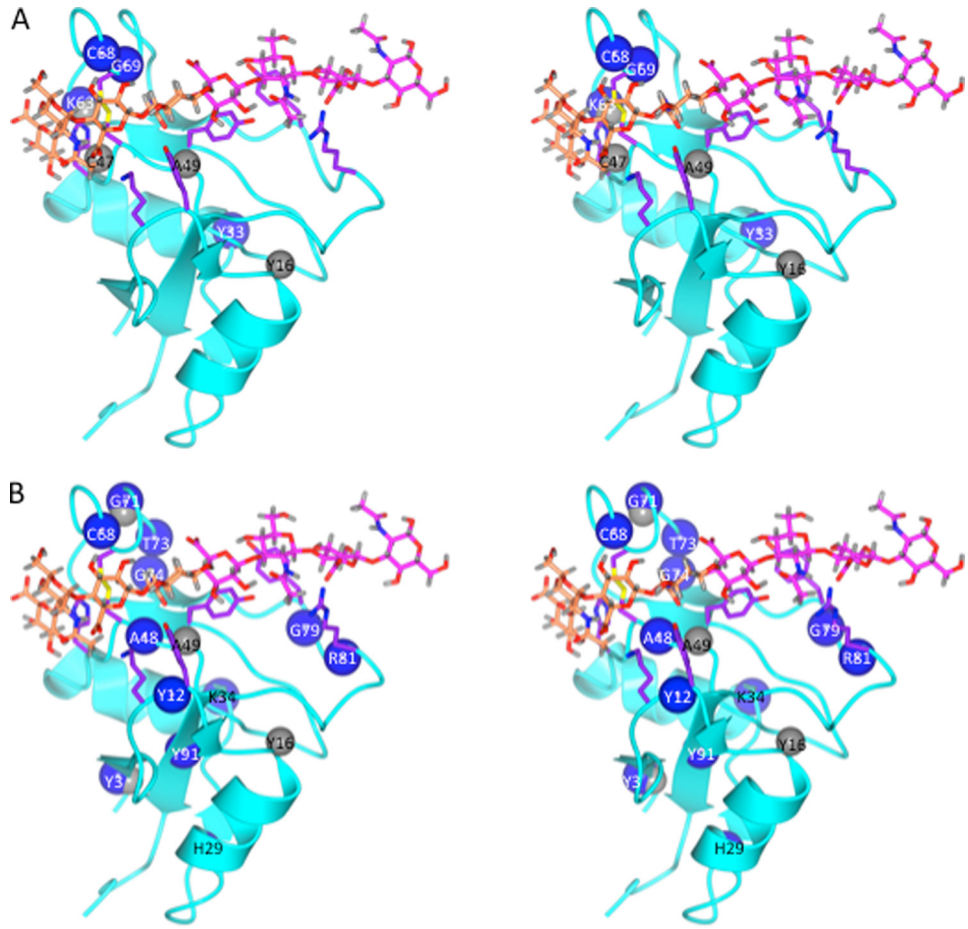

FIGURE 7. **Mapping of shift perturbations caused by hybrid oligomers HA_4C_4 and C_4HA_4 onto the refined Link_TSG6/HA_8^{AN} model.** *A* and *B*, stereoviews of the refined Link_TSG6/HA_8^{AN} model onto which the amide protons (*gray spheres*) and nitrogens (*blue spheres*) of Link_TSG6 determined to be significantly perturbed by HA_4C_4 (*A*) and C_4HA_4 (*B*), *i.e.* compared with chemical shift values in the presence of HA_8^{AN} (see Fig. 6), have been mapped. Amino acids implicated in mediating the interaction with HA are depicted in *purple*, whereas rings 1–4 and 5–8 of HA_8^{AN} are colored in *orange* and *pink*, respectively. In HA_4C_4 (*A*) the chondroitin sugars are positioned at the non-reducing end (*orange*), whereas C_4HA_4 (*B*) has its chondroitin sugars positioned at the reducing end (*pink*).

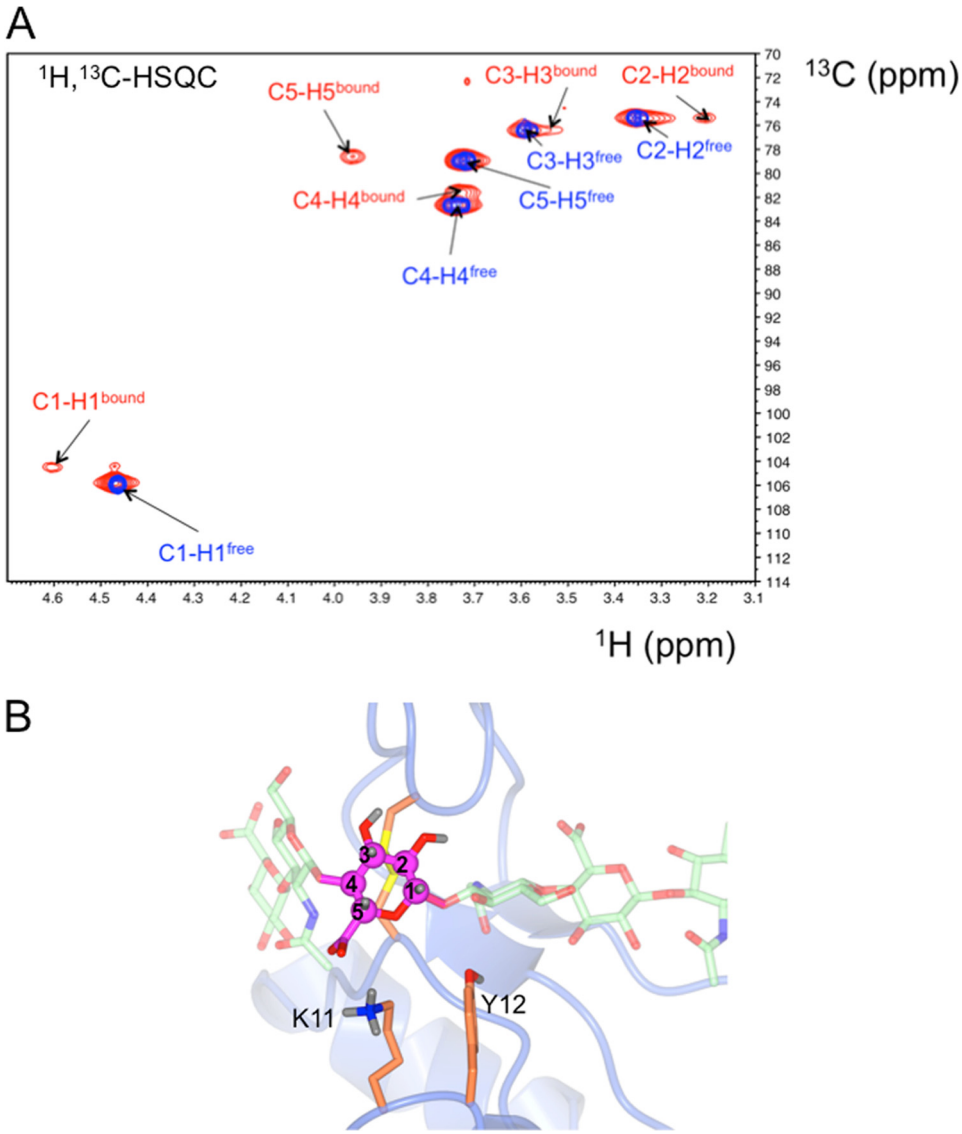

FIGURE 8. **Testing the Link_TSG6/HA$_8^{AN}$ model by NMR with a ^{13}C-labeled HA 8-mer.** *A*, an overlay of ^{13}C,^{1}H HSQC NMR spectra of an HA$_8^{AN}$-oligosaccharide in which ring 3 is uniformly ^{13}C-labeled (denoted *HA$_8^{AN}$-$^{13}C_6$-GlcUA3*) in the absence (*blue*) and presence (*red*) of unlabeled Link_TSG6 protein. *B*, the Link_TSG6/HA$_8^{AN}$ model showing the proximity of the labeled ring 3 carbons (*magenta*) to Lys^{11} and Tyr^{12} (*orange*); *e.g.* the large downfield shift of the H5 proton (*A*) may be caused by the formation of a salt-bridge between the carboxylate of GlcUA3 with the ϵ-NH_3^+ group of Lys^{11}.

predicted as only one face of GalNAc can make such a ring stacking interaction (due to steric hindrance of the other face by the axial C4-OH group). The other perturbations (to Tyr^3, His^{29}, Lys^{34}, and Tyr^{91}), although difficult to rationalize, may result from long-range conformational effects or C_4HA_4-induced changes in dynamics; *e.g.* we have described previously that Lys^{54}, although distant from the ligand binding groove, becomes less dynamic on interaction with HA (11).

The K_b of a chondroitin 8-mer was found to be ~20% of that for HA$_8^{AN}$. This indicates that when a GalNAc is present at all GlcNAc positions the combination of the deleterious effects seen for the hybrid oligomers (described above) causes a substantial reduction in affinity, in part due to the loss of favorable enthalpic interactions (see Table 1). This is perhaps because of the loss of hydrogen bonds between C4 hydroxyls on rings 4 and 6 and Tyr^{12} and Tyr^{78}, respectively; Ref. 10).

Interactions of Labeled-HA with Link_TSG6—A HA$_8^{AN}$ oligomer in which the ring 3 GlcUA was uniformly ^{13}C-labeled (denoted HA$_8^{AN}$-$^{13}C_6$-GlcUA3) was used to determine the effect of Link_TSG6 binding on the oligosaccharide (*i.e.* close to the position of the kink) and to provide independent information to test the refined model. Fig. 8*A* shows an overlay of ^{13}C,^{1}H HSQC spectra of the oligomer in the absence (*blue*) or presence (*red*) of unlabeled Link_TSG6, which indicates that the chemical shifts of the ring 3 C-H groups are all perturbed on binding to this protein; it should be noted that because the 8-mer is in more than a 3-fold excess over the protein, peaks are also present at the unbound positions in the latter spectra. Although the C3-H3 resonance only undergoes a relatively small change in chemical shift in the presence of Link_TSG6, the C1-H1, C2-H2, C4-H4, and C5-H5 groups all experience significant perturbations, *i.e.* C1-H1 (^{13}C, −1.30 ppm; ^{1}H, +0.14 ppm); C2-H2 (+0.07; −0.15); C3-H3 (−0.00; −0.06); C4-H4 (−1.05; −0.01); C5-H5 (−0.31; +0.23).

As can be seen from Fig. 8*B*, the highly perturbed C1-H1 and C5-H5 moieties are on one side of the sugar ring in close prox-

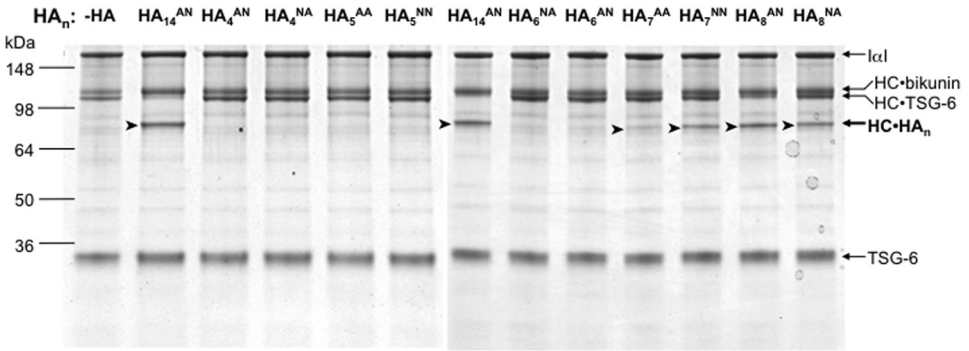

FIGURE 9. **Determining which HA oligomers act as substrates in heavy chain transfer.** SDS-PAGE analysis was used to determine the relative activities of 10 different HA$_n$ oligomers in the formation of TSG-6-mediated HC·HA$_n$ complexes in comparison with no added HA (−*HA*) and HA$_{14}^{AN}$ as a positive control. The relative positions of the HC·HA$_n$ reaction products (*arrowheads*), the bands corresponding to unreacted IαI and free TSG-6, the HC·TSG-6 complexes that act as intermediates in HC transfer, and HC·bikunin byproducts (as defined in Ref. 35) are all indicated on the *right hand side*.

imity to Lys^{11} and Tyr^{12} in the refined Link_TSG6/HA$_8^{AN}$ model; these amino acids have been found previously to be involved in mediating the interaction with HA based on mutagenesis and NMR analysis (10, 46, 47). Importantly, H5, which experiences the largest perturbation in ^{1}H chemical shift on Link_TSG6 binding (+0.23 ppm), is moved downfield, which is consistent with this proton being in proximity to Lys^{11} in the Link_TSG6/HA$_8^{AN}$ model (see Fig. 2). The C4 carbon is involved in the glycosidic bond linking rings 2 and 3, which is highly kinked such that the Φ/Ψ angles in the family of models, although favorable, occupy a limited region of the energy minima. Thus the distribution of conformations about the 2–3 glycosidic bond are likely to be distinct from those in free solution, which could account for the perturbation of the labeled C4 carbon in the NMR spectra (Fig. 8*A*). Furthermore, the H2 proton experiences a significant up field shift (−0.15 ppm), which perhaps could be explained by the proximity to Phe^{70} (in some models) that has been hypothesized previously to make an aromatic ring stacking interaction with ring 4 (17). Alternatively this perturbation (and the upfield shift changes to H3 and H4) could be due to their proximity to the electron-rich Cys^{47}-Cys^{68} disulfide bond.

Determining Which HA Oligomers Act as Substrates in Heavy Chain Transfer—Previously we showed that a HA$_{14}^{AN}$ oligosaccharide can act as a substrate in TSG-6-mediated heavy chain transfer, *i.e.* in the formation of a HC·HA complex (35). Here we assessed the relative activities of HA$_{14}^{AN}$ compared with the various HA oligomers employed within this study to determine the smallest HA oligosaccharide that can act as a substrate and to see if substrate efficiency correlates with affinity for Link_TSG6. From the representative SDS-PAGE analysis in Fig. 9, it can be observed that the reactions containing HA$_8^{AN}$, HA$_8^{NA}$, HA$_7^{NN}$, or HA$_7^{AA}$ all gave rise to visible bands of ~85 kDa, *i.e.* corresponding to HC·HA$_n$, whereas those with HA 4-, 5-, and 6-mers did not contain any clearly visible bands of this size. Thus, on the basis of these data the minimum size of HA oligosaccharide that can act as a substrate for heavy chain transfer is likely a 7-mer; it should be noted that previous work (on HA$_n^{AN}$ and HA$_n^{AA}$ oligomers) reported in Day *et al.* (71) indicated that HA$_5^{AA}$ may also act as a weak substrate; however, this finding was not reproduced here. As can be seen from Fig. 9, the HA$_8^{AN}$ was the preferred substrate for heavy chain transfer, giving the most intense HC·HA$_n$ band (although this was a slightly poorer substrate than the HA$_{14}^{AN}$ control), followed by HA$_8^{NA}$ and HA$_7^{NN}$ that gave similar amounts of product (*i.e.* approximately half that of HA$_8^{AN}$). HA$_7^{AA}$ also acted as a substrate, but transfer of HC onto this oligosaccharide appeared much less efficient (~10-fold less than for HA$_8^{AN}$). Interestingly, there appears to be no correlation between substrate efficiency of the 7- and 8-mers and the affinity of these oligomers for Link_TSG6 (see Table 1); *e.g.* the tightest binding oligomer HA$_8^{NA}$ is a weaker substrate than HA$_8^{AN}$, and the poor substrate HA$_7^{AA}$ has a similar affinity to HA$_8^{AN}$.

DISCUSSION

Here we have generated a refined model of the Link module from human TSG-6 in complex with a HA octasaccharide based on chemical shift maps for Link_TSG6 in the presence of defined HA oligomers of differing lengths; the use of HA oligosaccharides with GlcNAc at their reducing termini, not available until recently (52), has allowed the identification of novel structural restraints that were used to inform the modeling process. The model was also tested using new sugar reagents, *i.e.* hybrid HA oligosaccharides containing chondroitin disaccharide units and a HA 8-mer where only one sugar ring was isotopically labeled, that have not been described before. The refined model was found to be consistent with ITC and NMR data derived from experiments conducted with 13 distinct oligosaccharides.

Although the conformation and position of HA rings 3–8 are essentially identical to those in our original model (17), the novel interactions observed between ring 1 and the protein have allowed refinement of the Link_TSG6/HA$_8^{AN}$ complex such that this sugar makes close contacts with both Lys^{63} and His^{45}; both of these residues are completely conserved in the TSG-6 sequences from various species characterized to date (*e.g.* see alignment in Blundell *et al.* 60). Mutation of His^{45} has been shown previously to reduce the affinity of the interaction with HA$_8^{AN}$ by ~50% (60), which can now be explained by a subtle disruption of the ring stacking interaction between the histidine and GlcNAc2 when it is replaced with serine (Figs. 1 and 2).

Thus, in the new model the association of HA$_8^{AN}$ with Link_TSG6 is mediated by a combination of salt bridges, ring stack-

ing interactions, hydrogen bonds, and hydrophobic interactions where 7 of the 8 rings make contact with the protein surface (see Fig. 2); to utilize all of these interactions the HA must contact two faces of the Link module, which requires the glycosidic bonds between rings 2 and 3 and between rings 3 and 4, to be highly kinked. In this regard, NMR peaks II and III (*i.e.* arising from Val^{62} and Lys^{63}, respectively; Fig. 1) appear to be diagnostic for the presence of this kink in the HA chain (*i.e.* in HA_8^{AN}, HA_8^{NA}, HA_7^{NN}, HA_7^{AA}, and HA_6^{AN}), whereas peak IV may signal the formation of a partial kink, *i.e.* in the oligomers that have a reducing terminal GlcNAc lying in the ring 2 position, *e.g.* HA_6^{NA}, HA_5^{NN}, HA_4^{NA}; peak V likely identifies oligomers that do not kink (HA_5^{AA}, HA_4^{AN}) and thus do not make full contact with the His^{45} and Lys^{63} amino acids (see Fig. 2).

Based on our new modeling, HA_8^{AN} appears to be the minimum size of oligomer that can make the full complement of interactions with Link_TSG6 (Fig. 2); binding of HA_7^{AA}, although filling the binding site, is entropically unfavorable (Table 1). Moreover, the oligosaccharides with six or fewer sugars all have much lower affinities. The greatly decreased affinity of the hexasaccharides compared with HA_8^{AN} indicates that multiple interactions along both faces of the Link module surface are needed to generate the energy required to form the pronounced kink in the HA chain. Thus, once the interaction surface is long enough to induce the kink and overcome the "activation energy," a more favorable binding mode (and thus increased affinity) is attained.

However, it is not currently possible to fully rationalize the affinities of all the various HA oligomers on the basis of their proposed positions within the Link modules binding groove (Fig. 2). For example, determining a mechanism for the unusually high affinity observed for the interaction between Link_TSG6 and HA_8^{NA} is made more difficult by the observation that this oligosaccharide binds in two registers (see Fig. 2). It is possible that oligomer-specific "end effects" allow better matching of the HA dynamics with the dynamic motion of the protein (*e.g.* in the $\beta4$-$\beta5$ loop; Ref. 11) leading to a higher affinity; *e.g.* by enhancing the interactions between the reducing terminal GluUA and Arg^{81} (in the lower binding register shown in Fig. 2).

The refined Link_TSG6/HA_8^{AN} model suggests the formation of three salt bridges, *i.e.* between the carboxylate groups of the oligosaccharide rings 1, 3, and 7 and the side chains of Lys^{63}, Lys^{11}, and Arg^{81}, respectively (Fig. 2). Previous ITC data showed that on average the binding of Link_TSG6 to HA_8^{AN} only involves ~1.5 salt bridges (70), suggesting that these ionic interactions are transient. This is consistent with the finding that ionic interactions likely contribute only ~25% of the free energy of binding at physiological salt strengths (*i.e.* based on ITC measurements over a range of NaCl concentrations; Ref. 70) and also with the conclusion (here and in Refs. 10 and 17) that ring stacking and hydrogen bonds make a major contribution to binding.

As noted already, the HA chain in the refined Link_TSG6/HA_8^{AN} model is kinked and wraps around the protein surface. From Fig. 10 it can be seen that this is similar to the conformation of HA in the co-crystal structure of HA_8^{AN} bound to the HABD of CD44 (13). In both of these cases the HA octasaccharide is located in a similarly positioned binding groove on the Link module surface (Fig. 10*A*), although the kink in the CD44/HA complex is somewhat less pronounced (Fig. 10*B*); the HABD of CD44 is composed of additional N- and C-terminal segments that extend the Link module structure (12); however, these do not contribute significantly to the interaction with HA (13). Although there are clearly similarities in the manner in which the CD44 and TSG-6 interact with HA, the molecular details are quite distinct. For example, as described above, in the case of the refined Link_TSG6/HA_8^{AN} model 7, sugar rings make contact with the protein surface, whereas in CD44 only 5 rings are involved in binding (13). Furthermore, the interaction between Link_TSG6 and HA_8^{AN} is mediated in part by both ionic and ring stacking interactions (Fig. 2), whereas the binding of HA_8^{AN} to CD44 does not involve either of these types of interaction but rather is dominated by hydrogen bonds and van der Waals forces (13); the binding site in CD44, however, like TSG-6, does contain a hydrophobic pocket (in a position close to the well defined pocket in Link_TSG6 that is bounded by the Cys^{47}-Cys^{68} disulfide) that accommodates a methyl group of the HA. This large difference in the interaction networks of the Link_TSG6/HA_8^{AN} and HABD_CD44/HA_8^{AN} complexes probably explains why the binding of HA_8^{AN} to Link_TSG6 is of much higher affinity than that with HABD_CD44 when determined by ITC under similar conditions (*i.e.* K_d values of ~0.2 μM (Table 1) and ~125 μM (13), respectively). Overall, the TSG-6 Link module and its mode of HA association is expected to be more representative of the Link module family as a whole than CD44 (13, 17).

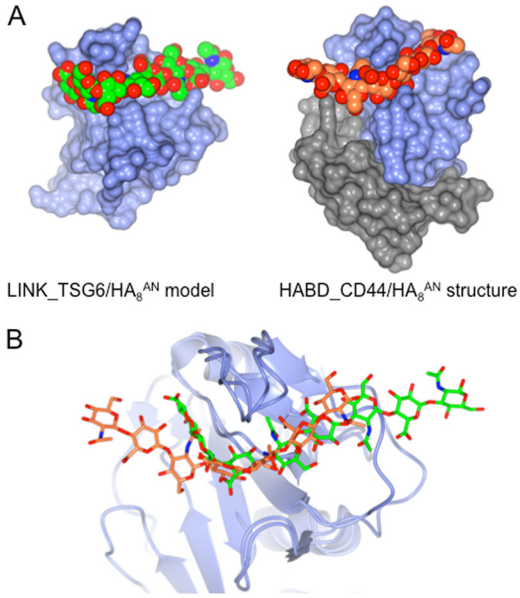

FIGURE 10. **Similarity of refined Link_TSG6/HA_8^{AN} model and the CD44/HA_8^{AN} co-complex.** *A*, a comparison of the Link_TSG6/HA_8^{AN} model (determined here) with the crystal structure of the HABD from murine CD44 in complex with HA_8^{AN} (13); the HA is shown in a space-filling representation where carbon atoms are colored *green* or *orange*, respectively. The proteins are represented as solvent-accessible surfaces, where the Link module domains, which are displayed in an equivalent orientation (based on an overlay of their secondary structures), are colored in *light blue*; in CD44, the N- and C-terminal segments that extend the Link module structure to form the larger HABD (12) are colored *gray*. *B*, an overlay of Link_TSG6/HA_8^{AN} and HABD_CD44/HA_8^{AN} with protein ribbons shown in *blue* and the HA shown in *green* (rings 1–8) and orange (rings 2–8), respectively.

These differences in the way that TSG-6 and CD44 interact with HA are perhaps not surprising given that the biological roles of these two proteins are so different. CD44 is a cell surface receptor that binds to HA through multiple weak interactions (72, 73), which can for example mediate rolling of leukocytes on the vascular endothelium (74–76); importantly, the low affinity and transient nature of the CD44/HA interaction has been found to be necessary for rolling to occur (77). On the other hand, TSG-6 has been demonstrated recently to form stable complexes with HA that cross-link this polysaccharide leading to the condensation of HA networks (29). This cross-linking may be important for the reorganization of extracellular matrix (*e.g.* at sites of inflammation where TSG-6 is expressed) and is also likely responsible for promoting the association of HA with CD44 on leukocytes (27–29). The recent observation that TSG-6 can decrease nuclear translocation of NF-κB in resident macrophages in a CD44-dependent manner (26) could also be explained by TSG-6-mediated cross-linking of HA (and thus enhanced receptor engagement) rather than by a direct interaction between TSG-6 and CD44 as has been suggested. In the study by Baranova *et al.* (29), both full-length TSG-6 and Link_TSG6 were found to be able to condense and rigidify HA networks even though the isolated Link module domain binds HA more weakly (and non-cooperatively) compared with the intact protein. This condensation of HA could potentially be explained, at least in part, by the pronounced kink that our refined model predicts to be induced in the HA chain on binding to the TSG-6 Link module (*i.e.* leading to an apparent chain shortening).

As described under "Results," Link_TSG6 can bind to a chondroitin 8-mer with an ~5-fold lower affinity compared with that of HA_8^{AN}; based on the experiments with the hybrid oligomers, this non-sulfated glycosaminoglycan can be accommodated within the Link module HA-binding groove. The finding that the NMR shift perturbations for Link_TSG6 in the presence of these hybrid oligosaccharides were only subtly different compared with HA_8^{AN} suggests that TSG-6 is also likely to induce a bent conformation in chondroitin. If this is the case, then the binding of TSG-6 to unsulfated stretches of chondroitin sulfate may be able to condense this glycosaminoglycan (*i.e.* as we have observed for HA; Ref. 29) and could serve to contract the overall domain size of a chondroitin-sulfate proteoglycan. This could have pronounced effects on the organization of extracellular matrices (*e.g.* leading to more condensed matrix structures) and might also enhance the movement of chondroitin-sulfate proteoglycans within tissues, *e.g.* aiding the diffusion of *de novo* synthesized aggrecan out of the chondrocyte pericellular matrix during cartilage remodeling; such activities could be envisaged to contribute to TSG-6 chondroprotective function.

The new model of the Link_TSG6/HA_8^{AN} complex potentially has implications for understanding the mechanism underlying TSG-6-mediated heavy chain transfer onto HA; TSG-6 has been demonstrated to form covalent complexes with both HC1 and HC2 (*i.e.* HC1·TSG-6 and HC2·TSG-6 (35, 39) that act as intermediates in the formation of HC·HA (35). In this regard a serine residue in the N-terminal region of TSG-6 (*i.e.* Ser^{28} using the numbering for the full-length preprotein (48), in which the first amino acid of the Link_TSG6 would be at sequence position 36) has been shown to form an ester bond with the C-terminal aspartic acid residues of the heavy chains (40); the ester bond in an HC·TSG-6 complex is then transferred from TSG-6 onto the C6 hydroxyl of a GlcNAc sugar in HA (see Ref. 35). Therefore, it is conceivable that HA recognition during the HC transfer reaction could involve the binding of HA to the Link module of TSG-6 (*i.e.* where the HA adopts the conformation in our model). However, this scenario seems unlikely given that there was no correlation between the substrate activities of various HA oligomers and their affinities for Link_TSG6 (*e.g.* HA_7^{AA} was a much poorer substrate than HA_8^{AN} while having similar binding constants; Table 1 and Fig. 9). This observation suggests that the binding site for HA in the context of an HC·TSG-6 complex may be distinct from that in free TSG-6. Consistent with this hypothesis, we have found that the interaction between TSG-6 and IαI (and the formation of the HC·TSG-6 complex) inhibits the binding of HA to TSG-6 (28); this prevents TSG-6-mediated cross-linking of HA and can abolish the enhancement of HA binding to cell surface CD44. Thus the interaction of HC with TSG-6 likely occludes the HA-binding site in TSG-6 or stabilizes the Link module in its closed conformation; either way this would prevent some or all of the HA-binding residues described here from interacting with HA. In this regard we have found that a mutant of full-length TSG-6 (where Tyr^{94} (equivalent to Tyr^{59} in Link_TSG6) was mutated to phenylalanine), with greatly impaired HA-binding activity,[6] is able to mediate HC transfer (78). Further work is now necessary to determine whether the HA-binding groove that we have defined in the Link_TSG6/HA_8^{AN} complex plays any role in the formation of HC·HA complexes.

In summary, we have used experimental data derived from a series of 13 defined and distinct oligosaccharides to build a refined model of an HA octasaccharide in complex with the TSG-6 Link module domain. This model has provided new insights into the molecular basis of HA/protein interactions and is helpful in furthering our understanding of the functional role of TSG-6 in extracellular matrix reorganization.

Acknowledgment—We thank Professor Erik Fries for providing the IαI protein used in this study.

REFERENCES

1. Tammi, M. I., Day, A. J., and Turley, E. A. (2002) Hyaluronan and homeostasis. A balancing act. *J. Biol. Chem.* **277,** 4581–4584
2. Toole, B. P., Wight, T. N., and Tammi, M. I. (2002) Hyaluronan-cell interactions in cancer and vascular disease. *J. Biol. Chem.* **277,** 4593–4596
3. Itano, N. (2008) Simple primary structure, complex turnover regulation and multiple roles of hyaluronan. *J. Biochem.* **144,** 131–137
4. Jiang, D., Liang, J., and Noble, P. W. (2011) Hyaluronan as an immune regulator in human diseases. *Physiol. Rev.* **91,** 221–264
5. Day, A. J., and Sheehan, J. K. (2001) Hyaluronan: Polysaccharide chaos to protein organisation. *Curr. Opin. Struct. Biol.* **11,** 617–622
6. Day, A. J., and de la Motte, C. A. (2005) Hyaluronan cross-linking: A protective mechanism in inflammation? *Trends Immunol.* **26,** 637–643
7. Day, A. J., and Prestwich, G. D. (2002) Hyaluronan-binding proteins: Ty-

[6] M. R. Rugg and A. J. Day, unpublished data.

ing up the giant. *J. Biol. Chem.* **277,** 4585–4588
8. Blundell, C. D., Seyfried, N. T., and Day, A. J. (2004) Structural and functional diversity of hyaluronan-binding proteins. In *Chemistry and Biology of Hyaluronan* (Garg, H. G., and Hales, C. A., eds) pp. 189–204, Elsevier Science Publishing Co., Inc., New York
9. Kohda, D., Morton, C. J., Parkar, A. A., Hatanaka, H., Inagaki, F. M., Campbell, I. D., and Day, A. J. (1996) Solution structure of the link module: A hyaluronan-binding domain involved in extracellular matrix stability and cell migration. *Cell* **86,** 767–775
10. Blundell, C. D., Mahoney, D. J., Almond, A., DeAngelis, P. L., Kahmann, J. D., Teriete, P., Pickford, A. R., Campbell, I. D., and Day, A. J. (2003) The link module from ovulation- and inflammation-associated protein TSG-6 changes conformation on hyaluronan binding. *J. Biol. Chem.* **278,** 49261–49270
11. Higman, V. A., Blundell, C. D., Mahoney, D. J., Redfield C., Noble, M. E., and Day, A. J. (2007) Plasticity of the TSG-6 HA-binding loop and mobility in the TSG-6-HA complex revealed by NMR and x-ray crystallography. *J. Mol. Biol.* **371,** 669–684
12. Teriete, P., Banerji, S., Noble, M., Blundell, C. D., Wright, A. J., Pickford, A. R., Lowe, E., Mahoney, D. J., Tammi, M. I., Kahmann, J. D., Campbell, I. D., Day, A. J., and Jackson, D. G. (2004) Structure of the regulatory hyaluronan binding domain in the inflammatory leukocyte homing receptor CD44. *Mol. Cell* **13,** 483–496
13. Banerji, S., Wright, A. J., Noble, M., Mahoney, D. J., Campbell, I. D., Day, A. J., and Jackson, D. G. (2007) Structures of the Cd44-hyaluronan complex provide insight into a fundamental carbohydrate-protein interaction. *Nat. Struct. Mol. Biol.* **14,** 234–239
14. Banerji, S., Hide, B. R., James, J. R., Noble, M. E., and Jackson, D. G. (2010) Distinctive properties of the hyaluronan-binding domain in the lymphatic endothelial receptor Lyve-1 and their implications for receptor function. *J. Biol. Chem.* **285,** 10724–10735
15. Matsumoto, K., Shionyu, M., Go, M., Shimizu, K., Shinomura, T., Kimata, K., and Watanabe, H. (2003) Distinct interaction of versican/PG-M with hyaluronan and link protein. *J. Biol. Chem.* **278,** 41205–41212
16. Seyfried, N. T., McVey, G. F., Almond, A., Mahoney, D. J., Dudhia, J., and Day, A. J. (2005) Expression and purification of functionally active hyaluronan-binding domains from human cartilage link protein, aggrecan, and versican. Formation of ternary complexes with defined hyaluronan oligosaccharides. *J. Biol. Chem.* **280,** 5435–5448
17. Blundell, C. D., Almond, A., Mahoney, D. J., DeAngelis, P. L., Campbell, I. D., and Day, A. J. (2005) Towards a structure for a TSG-6.hyaluronan complex by modeling and NMR spectroscopy. Insights into other members of the link module superfamily. *J. Biol. Chem.* **280,** 18189–18201
18. Milner, C. M., and Day, A. J. (2003) TSG-6: A multifunctional protein associated with inflammation. *J. Cell Sci.* **116,** 1863–1873
19. Milner, C. M., Higman, V. A., and Day, A. J. (2006) TSG-6: A pluripotent inflammatory mediator? *Biochem. Soc. Trans.* **34,** 446–450
20. Szántó, S., Bárdos, T., Gál, I., Glant, T. T., and Mikecz, K. (2004) Enhanced neutrophil extravasation and rapid progression of proteoglycan-induced arthritis in TSG-6-knockout mice. *Arthritis Rheum.* **50,** 3012–3022
21. Nagyeri, G., Radacs, M., Ghassemi-Nejad, S., Tryniszewska, B., Olasz, K., Hutas, G., Gyorfy, Z., Hascall, V. C., Glant, T. T., and Mikecz, K. (2011) TSG-6 protein, a negative regulator of inflammatory arthritis, forms a ternary complex with murine mast cell tryptases and heparin. *J. Biol. Chem.* **286,** 23559–23569
22. Mahoney, D. J., Mikecz, K., Ali, T., Mabilleau, G., Benayahu, D., Plaas, A., Milner, C. M., Day, A. J., and Sabokbar, A. (2008) TSG-6 regulates bone remodeling through inhibition of osteoblastogenesis and osteoclast activation. *J. Biol. Chem.* **283,** 25952–25962
23. Mahoney, D. J., Swales, C., Athanasou, N. A., Bombardieri, M., Pitzalis, C., Kliskey, K., Sharif, M., Day, A. J., Milner, C. M., and Sabokbar, A. (2011) TSG-6 inhibits osteoclast activity via an autocrine mechanism and is functionally synergistic with osteoprotegerin. *Arthritis Rheum.* **63,** 1034–1043
24. Lee, R. H., Pulin, A. A., Seo, M. J., Kota, D. J., Ylostalo, J., Larson, B. L., Semprun-Prieto, L., Delafontaine, P., and Prockop, D. J. (2009) Intravenous hMSCs improve myocardial infarction in mice because cells embolized in lung are activated to secrete the anti-inflammatory protein TSG-6. *Cell Stem Cell* **5,** 54–63
25. Oh, J. Y., Roddy, G. W., Choi, H., Lee, R. H., Ylöstalo, J. H., Rosa, R. H. Jr., and Prockop, D. J. (2010) Anti-inflammatory protein TSG-6 reduces inflammatory damage to the cornea following chemical and mechanical injury. *Proc. Natl. Acad. Sci. U.S.A.* **107,** 16875–16880
26. Choi, H., Lee, R. H., Bazhanov, N., Oh, J. Y., and Prockop, D. J. (2011) Anti-inflammatory protein TSG-6 secreted by activated MSCs attenuates zymosan-induced mouse peritonitis by decreasing TLR2/NF-κB signaling in resident macrophages. *Blood* **118,** 330–338
27. Lesley, J., Gál, I., Mahoney, D. J., Cordell, M. R., Rugg, M. S., Hyman, R., Day, A. J., and Mikecz, K. (2004) TSG-6 modulates the interaction between hyaluronan and cell surface CD44. *J. Biol. Chem.* **279,** 25745–25754
28. Baranova, N. S., Foulcer, S. J., Briggs, D. C., Tilakaratna, V., Enghild, J. J., Milner, C. M., Day, A. J., and Richter, R. P. (2013) Inter-α-inhibitor impairs TSG-6-induced hyaluronan cross-linking. *J. Biol. Chem.* **288,** 29642–29653
29. Baranova, N. S., Nilebäck, E., Haller, F. M., Briggs, D. C., Svedhem, S., Day, A. J., and Richter, R. P. (2011) The inflammation-associated protein TSG-6 cross-links hyaluronan via hyaluronan-induced TSG-6 oligomers. *J. Biol. Chem.* **286,** 25675–25686
30. Fülöp, C., Szántó, S., Mukhopadhyay, D., Bárdos, T., Kamath, R. V., Rugg, M. S., Day, A. J., Salustri, A., Hascall, V. C., Glant, T. T., and Mikecz, K. (2003) Impaired cumulus mucification and female sterility in tumor necrosis factor-induced protein-6 deficient mice. *Development* **130,** 2253–2261
31. Ochsner, S. A., Day, A. J., Rugg, M. S., Breyer, R. M., Gomer, R. H., and Richards, J. S. (2003) Disrupted function of tumor necrosis factor-α-stimulated gene 6 blocks cumulus cell-oocyte complex expansion. *Endocrinology* **144,** 4376–4384
32. Zhao, M., Yoneda, M., Ohashi, Y., Kurono, S., Iwata, H., Ohnuki, Y., and Kimata, K. (1995) Evidence for the covalent binding of SHAP, heavy chains of inter-α-trypsin inhibitor, to hyaluronan. *J. Biol. Chem.* **270,** 26657–26663
33. Zhuo, L., Yoneda, M., Zhao, M., Yingsung, W., Yoshida, N., Kitagawa, Y., Kawamura, K., Suzuki, T., and Kimata, K. (2001) Defect in SHAP-hyaluronan complex causes severe female infertility. A study by inactivation of the bikunin gene in mice. *J. Biol. Chem.* **276,** 7693–7696
34. Sato, H., Kajikawa, S., Kuroda, S., Horisawa, Y., Nakamura, N., Kaga, N., Kakinuma, C., Kato, K., Morishita, H., Niwa, H., and Miyazaki, J. (2001) Impaired fertility in female mice lacking urinary trypsin inhibitor. *Biochem. Biophys. Res. Comm.* **281,** 1154–1160
35. Rugg, M. S., Willis, A. C., Mukhopadhyay, D., Hascall, V. C., Fries, E., Fülöp, C., Milner, C. M., and Day, A. J. (2005) Characterization of complexes formed between TSG-6 and inter-α-inhibitor that act as intermediates in the covalent transfer of heavy chains onto hyaluronan. *J. Biol. Chem.* **280,** 25674–25686
36. Wisniewski, H. G., Maier, R., Lotz, M., Lee, S., Klampfer, L., Lee, T. H., and Vilcek, J. (1993) TSG-6. A TNF-, IL-1-, and LPS-inducible secreted glycoprotein associated with arthritis. *J. Immunol.* **151,** 6593–6601
37. Yingsung, W., Zhuo, L., Morgelin, M., Yoneda, M., Kida, D., Watanabe, H., Ishiguro, N., Iwata, H., and Kimata, K. (2003) Molecular heterogeneity of the SHAP-hyaluronan complex. Isolation and characterization of the complex in synovial fluid from patients with rheumatoid arthritis. *J. Biol. Chem.* **278,** 32710–32718
38. Forteza, R., Casalino-Matsuda, S. M., Monzon, M. E., Fries, E., Rugg, M. S., Milner, C. M., and Day, A. J. (2007) TSG-6 potentiates the antitissue kallikrein activity of inter-α-inhibitor through bikunin release. *Am. J. Respir. Cell Mol. Biol.* **36,** 20–31
39. Sanggaard, K. W., Karring, H., Valnickova, Z., Thøgersen, I. B., and Enghild, J. J. (2005) The TSG-6 and IαI interaction promotes a transesterification cleaving the protein-glycosaminoglycan-protein (PGP) cross-link. *J. Biol. Chem.* **280,** 11936–11942
40. Sanggaard, K. W., Sonne-Schmidt, C. S., Krogager, T. P., Kristensen, T., Wisniewski, H. G., Thøgersen, I. B., and Enghild, J. J. (2008) TSG-6 transfers proteins between glycosaminoglycans via a Ser-28-mediated covalent catalytic mechanism. *J. Biol. Chem.* **283,** 33919–33926
41. Salustri, A., Garlanda, C., Hirsch, E., De Acetis, M., Maccagno, A., Bottazzi, B., Doni, A., Bastone, A., Mantovani, G., Beck Peccoz, P., Salvatori,

G., Mahoney, D. J., Day, A. J., Siracusa, G., Romani, L., and Mantovani, A. (2004) PTX3 plays a key role in the organization of the cumulus oophorus extracellular matrix and in *in vivo* fertilization. *Development* **131,** 1577–1586

42. Ievoli, E., Lindstedt, R., Inforzato, A., Camaioni, A., Palone, F., Day, A. J., Mantovani, A., Salvatori, G., and Salustri, A. (2011) Implication of the oligomeric state of the N-terminal PTX3 domain in cumulus matrix assembly. *Matrix Biol.* **30,** 330–337
43. Inforzato, A., Baldock, C., Jowitt, T. A., Holmes, D. F., Lindstedt, R., Marcellini, M., Rivieccio, V., Briggs, D. C., Kadler, K. E., Verdoliva, A., Bottazzi, B., Mantovani, A., Salvatori, G., and Day, A. J. (2010) The angiogenic inhibitor long pentraxin PTX3 forms an asymmetric octamer with two binding sites for FGF2. *J. Biol. Chem.* **285,** 17681–17692
44. Inforzato, A., Rivieccio, V., Morreale, A. P., Bastone, A., Salustri, A., Scarchilli, L., Verdoliva, A., Vincenti, S., Gallo, G., Chiapparino, C., Pacello, L., Nucera, E., Serlupi-Crescenzi, O., Day, A. J., Bottazzi, B., Mantovani, A., De Santis, R., and Salvatori, G. (2008) Structural characterization of PTX3 disulfide bond network and its multimeric status in cumulus matrix organization. *J. Biol. Chem.* **283,** 10147–10161
45. Scarchilli, L., Camaioni, A., Bottazzi, B., Negri, V., Doni, A., Deban, L., Bastone, A., Salvatori, G., Mantovani, A., Siracusa, G., and Salustri, A. (2007) PTX3 interacts with inter-α-trypsin inhibitor. Implications for hyaluronan organization and cumulus oophorus expansion. *J. Biol. Chem.* **282,** 30161–30170
46. Mahoney, D. J., Blundell, C. D., and Day, A. J. (2001) Mapping the hyaluronan-binding site on the link module from human tumor necrosis factor-stimulated gene-6 by site-directed mutagenesis. *J. Biol. Chem.* **276,** 22764–22771
47. Getting, S. J., Mahoney, D. J., Cao, T., Rugg, M. S., Fries, E., Milner, C. M., Perretti, M., and Day, A. J. (2002) The link module from human TSG-6 inhibits neutrophil migration in a hyaluronan- and inter-α-inhibitor-independent manner. *J. Biol. Chem.* **277,** 51068–51076
48. Lee, T. H., Wisniewski, H. G., and Vilcek, J. (1992) A novel secretory tumor necrosis factor-inducible protein (TSG-6) is a member of the family of hyaluronate binding proteins, closely related to the adhesion receptor CD44. *J. Cell Biol.* **116,** 545–557
49. Day, A. J., Aplin, R. T., and Willis, A. C. (1996) Overexpression, purification, and refolding of link module from human TSG-6 in *Escherichia coli*. Effect of temperature, media, and mutagenesis on lysine misincorporation at arginine AGA codons. *Protein Expr. Purif.* **8,** 1–16
50. Kahmann, J. D., Koruth, R., and Day, A. J. (1997) Method for quantitative refolding of the link module from human TSG-6. *Protein Expr. Purif.* **9,** 315–318
51. Kahmann, J. D., O'Brien, R., Werner, J. M., Heinegârd, D., Ladbury, J. E., Campbell, I. D., and Day, A. J. (2000) Localization and characterization of the hyaluronan-binding site on the link module from human TSG-6. *Structure* **8,** 763–774
52. Blundell, C. D., and Almond, A. (2006) Enzymatic and chemical methods for the generation of pure hyaluronan oligosaccharides with both odd and even numbers of monosaccharide units. *Anal. Biochem.* **353,** 236–247
53. Tracy, B. S., Avci, F. Y., Linhardt, R. J., and DeAngelis, P. L. (2007) Acceptor specificity of the *Pasteurella* hyaluronan and chondroitin synthases and production of chimeric glycosaminoglycans. *J. Biol. Chem.* **282,** 337–344
54. DeAngelis, P. L., Oatman, L. C., and Gay, D. F. (2003) Rapid chemoenzymatic synthesis of monodisperse hyaluronan oligosaccharides with immobilized enzyme reactors. *J. Biol. Chem.* **278,** 35199–35203
55. DeAngelis, P. L., Gunay, N. S., Toida, T., Mao, W.-J., and Linhardt, R. J. (2002) Identification of the capsular polysaccharides of Type D and F *Pasteurella multocida* as unmodified heparin and chondroitin, respectively. *Carbohydr. Res.* **337,** 1547–1552
56. Mahoney, D. J., Aplin, R. T., Calabro, A., Hascall, V. C., and Day, A. J. (2001) Novel methods for the preparation and characterization of hyaluronan oligosaccharides of defined length. *Glycobiology* **11,** 1025–1033
57. Dougherty, B. A., and van de Rijn, I. (1993) Molecular characterization of hasB from an operon required for hyaluronic acid synthesis in group A streptococci. Demonstration of UDP-glucose dehydrogenase activity. *J. Biol. Chem.* **268,** 7118–7124
58. Delaglio, F., Grzesiek, S., Vuister, G. W., Zhu, G., Pfeifer, J., and Bax, A. (1995) NMRPipe. A multidimensional spectral processing system based on UNIX pipes. *J. Biomol. NMR* **6,** 277–293
59. Blundell, C. D., Reed, M. A., Overduin, M., and Almond, A. (2006) NMR spectra of oligosaccharides at ultra-high field (900 MHz) have better resolution than expected due to favourable molecular tumbling. *Carbohydr. Res.* **341,** 1985–1991
60. Blundell, C. D., Mahoney, D. J., Cordell, M. R., Almond, A., Kahmann, J. D., Perczel, A., Taylor, J. D., Campbell, I. D., and Day, A. J. (2007) Determining the molecular basis for the pH-dependent interaction between the link module of human TSG-6 and hyaluronan. *J. Biol. Chem.* **282,** 12976–12988
61. Nentwich, H. A., Mustafa, Z., Rugg, M. S., Marsden, B. D., Cordell, M. R., Mahoney, D. J., Jenkins, S. C., Dowling, B., Fries, E., Milner, C. M., Loughlin, J., and Day, A. J. (2002) A novel allelic variant of the human TSG-6 gene encoding an amino acid difference in the CUB module. Chromosomal localization, frequency analysis, modeling, and expression. *J. Biol. Chem.* **277,** 15354–15362
62. Blom, A., Pertoft, H., and Fries, E. (1995) Inter-α-inhibitor is required for the formation of the hyaluronan-containing coat on fibroblasts and mesothelial cells. *J. Biol. Chem.* **270,** 9698–9701
63. McGaughey, G. B., Gagné, M., and Rappé, A. K. (1998) pi-Stacking interactions. Alive and well in proteins. *J. Biol. Chem.* **273,** 15458–15463
64. Churchill, C. D., and Wetmore, S. D. (2009) Noncovalent interactions involving histidine. The effect of charge on pi-pi stacking and T-shaped interactions with the DNA nucleobases. *J. Phys. Chem. B* **113,** 16046–16058
65. Almond, A., Sheehan, J. K., and Brass, A. (1997) Molecular dynamics simulations of the two disaccharides of hyaluronan in aqueous solution. *Glycobiology* **7,** 597–604
66. Almond, A., Brass, A., and Sheehan, J. K. (1998) Dynamic exchange between stabilized conformations predicted for hyaluronan tetrasaccharides. Comparison of molecular dynamics simulations with available NMR data. *Glycobiology* **8,** 973–980
67. Almond, A., Brass, A., and Sheehan, J. K. (2000) Oligosaccharides as model systems for understanding water-biopolymer interaction. Hydrated dynamics of a hyaluronan decamer. *J. Phys. Chem. B* **104,** 5634–5640
68. Yamashita, S., Yoshida, H., Uchiyama, Y., Nakakita, Y., Nakakita, S., Tonozuka, T., Oguma, K., Nishikawa, A., and Kamitori, S. (2012) Carbohydrate recognition mechanism of HA70 from *Clostridium botulinum* deduced from x-ray structures in complexes with sialylated oligosaccharides. *FEBS Lett.* **586,** 2402–2410
69. Chodera, J. D., and Mobley, D. L. (2013) Entropy-enthalpy compensation. Role and ramifications in biomolecular ligand recognition and design. *Annu. Rev. Biophys.* **42,** 121–142
70. Blundell, C. D., Kahmann, J. D., Perczel, A., Mahoney, D. J., Cordell, M. R., Teriete, P., Campbell, I. D., and Day, A. J. (2002) Getting to grips with HA-protein interactions. In *Hyaluronan* (Kennedy, J. F., Phillips, G. O., Williams, P. A., and Hascall, V. C., eds) Vol. 1, pp. 161–172, Woodhead Publishing Ltd., Abington, Cambridge, UK
71. Day, A. J., Rugg, M. S., Mahoney, D. J., and Milner, C. M. (2004) The role of hyaluronan-binding proteins in ovulation. In *Hyaluronan: Structure, Metabolism, Biological Activities, Therapeutic Applications* (Balazs, E. A., and Hascall, V. C., eds) Vol. II, pp. 675–686, Matrix Biology Institute, Edgewater, NJ
72. Lesley, J., Hascall, V. C., Tammi, M., and Hyman, R. (2000) Hyaluronan binding by cell surface CD44. *J. Biol. Chem.* **275,** 26967–26975
73. Wolny, P. M., Banerji, S., Gounou, C., Brisson, A. R., Day, A. J., Jackson, D. G., and Richter, R. P. (2010) Analysis of CD44-hyaluronan interactions in an artificial membrane system. Insights into the distinct binding properties of high and low molecular weight hyaluronan. *J. Biol. Chem.* **285,** 30170–30180
74. Mohamadzadeh, M., DeGrendele, H., Arizpe, H., Estess, P., and Siegelman, M. (1998) Proinflammatory stimuli regulate endothelial hyaluronan expression and CD44/HA-dependent primary adhesion. *J. Clin. Invest.* **101,** 97–108
75. Nandi, A., Estess, P., and Siegelman, M. H. (2000) Hyaluronan anchoring and regulation on the surface of vascular endothelial cells is mediated

through the functionally active form of CD44. *J. Biol. Chem.* **275,** 14939–14948
76. Siegelman, M. H., DeGrendele, H. C., and Estess, P. (1999) Activation and interaction of CD44 and hyaluronan in immunological systems. *J. Leukoc. Biol.* **66,** 315–321
77. Lesley, J., English, N. M., Gál, I., Mikecz, K., Day, A. J., and Hyman, R. (2002) Hyaluronan binding properties of a CD44 chimera containing the link module of TSG-6. *J. Biol. Chem.* **277,** 26600–26608
78. Selbi, W., Day, A. J., Rugg, M. S., Fülöp, C., de la Motte, C. A., Bowen, T., Hascall, V. C., and Phillips, A. (2006) Overexpression of hyaluronan synthase 2 alters hyaluronan distribution and function in proximal tubular epithelial cells. *J. Am. Soc. Nephrol.* **17,** 1553–1567